TEMPERATURE DEPENDENCE OF MOLECULAR PHOSPHORESCENCE

By
WILLIAM EMIL MOEHLE

A DISSERTATION PRESENTED TO THE GRADUATE COUNCIL
OF THE UNIVERSITY OF FLORIDA
IN PARTIAL FULFILLMENT OF THE REQUIREMENTS FOR THE
DEGREE OF DOCTOR OF PHILOSOPHY

UNIVERSITY OF FLORIDA

1975

To my parents

ACKNOWLEDGEMENTS

I wish to express my appreciation to Dr. Martin T. Vala for his advice and encouragement throughout this work. His many suggestions and comments on this project were of inestimable value.

While there are many people who have helped and encouraged me in this work, special thanks and gratitude are due Neil Weinstein, Arleen French, and Ann Kennedy for their extraordinary efforts in helping me through the harder moments of this project. Special thanks are also due the members of Dr. Vala's research group, particularly Joseph Baiardo, Ralph Spafford, and Joseph Wrobel, the Electronics Shop, who were especially helpful on the technical side of my work, and Ken Wagener and Dick and Barbara Galley, whose friendship has been a particular source of strength.

Finally, I wish to mention again Ann Kennedy who performed a major miracle in getting this manuscript finished on time.

TABLE OF CONTENTS

LIST OF TABLES

LIST OF FIGURES

Abstract of Dissertation Presented to the
Graduate Council of the University of Florida
in Partial Fulfillment of the Requirements for
the Degree of Doctor of Philosophy

TEMPERATURE DEPENDENCE OF
MOLECULAR PHOSPHORESCENCE

By

William Emil Moehle

December, 1975

Chairman: Martin T. Vala
Major Department: Chemistry

Phosphorescence emission has been used as a probe for studying the triplet manifold of two molecular systems. For the first, we have observed the phosphorescence decay times of the benzene:chloroform:alkane system as a function of temperature. We have fit the results to a number of different rate equations and used the parameters thus obtained to elucidate the radiationless processes in benzene. To account for the data, we propose that an exciplex is formed between triplet benzene, chloroform and solvent. This model provides a framework for understanding a wide variety of photochemistry involving benzene in different phases. Calculations have been performed using open and closed shell INDO semi-empirical theories that show the validity of our arguments and shed additional light on the structure of the exciplex.

For the second system, duraldehyde in durene, we have studied in detail the temperature dependence of both the phosphorescence lifetime and intensity. We have further observed the temperature dependence of the infrared spectrum in the critical carbonyl stretching region and have observed the effects of ultraviolet photolysis on the intensity of these bands. From these data we have formulated a coherent kinetic model for the dissipation of triplet energy which is consistent with previous results. Finally, we have proposed a comprehensive model which describes all known photophysical and photochemical processes occurring via the duraldehyde triplet manifold.

CHAPTER I
INTRODUCTION

Background

It has been known for a long time[1] that many molecules exhibit long-lived emission (phosphorescence) after electronic excitation. As early as 1935, Jablonski[2] suggested a triplet state as the metastable species involved. In 1944, Lewis and Kasha[3] reported the results of the first extensive study of the emission from these metastable species and in the following year Lewis and Calvin[4] showed that this species was paramagnetic. Actually, it wasn't until 1958 and the photo-excited ESR experiments on naphthalene in durene that Hutchinson and Magnum[5] proved that this state was indeed a triplet.

Since that time there have been many studies undertaken that have used phosphorescent emission as a probe to study the triplet manifold of molecular systems.[6] Benzene - along with its simple derivatives - and aromatic carbonyls are two classes of compounds that have received considerable attention. It is the intent of this dissertation to further our understanding of both these classes of compounds. For the first class, we have studied the phosphorescence characteristics of a weak benzene complex, while for the second class we have studied the phosphorescence characteristics and ground state infrared of the system duraldehyde in durene.

While each of these studies is essentially independent of the other, they do share a number of common features among which is a general understanding of the problem of decay from an excited state.

The Phosphorescence Decay Problem

If an excited level of a molecular ensemble has a larger population than permitted by normal thermal excitation, then that state will attempt to lose this excess population by any means available. For the simplest situation involving the triplet manifold, this means that molecules in the lowest triplet state (T_1) will revert to the molecular ground state (S_0) by either (or both) radiative or nonradiative transitions. Thus the decay of T_1 is described by:

$$\frac{d[T_1]}{dt} = -(k_{10}^{r} + k_{10}^{nr})\ [T_1] \qquad (1)$$

where t = time

$[T_1]$ = population of T_1 at any time

r = radiative transition

nr = nonradiative transition

k_{10} = rate constant for the $T_1 \rightarrow S_o$ transition

The solution of this problem is:

$$[T_1] = [T_1]_0\ e^{-k_{10}t} \qquad (2)$$

where $k_{10} = k_{10}^{nr} + k_{10}^{r}$

$[T_1]_0$ = population of T_1 at $t = 0$

and hence, we are dealing with a simple exponential decay.

The triplet manifold of a molecule is rarely this simple.

The triplet state consists of two unpaired electrons which make it highly reactive, and the spin forbidden nature of the transition to the ground state makes the triplet state a long-lived species. Actually, all the familiar processes of complex formation, chemical reaction, isomerization, etc. may occur in the triplet manifold. It is frequently difficult to decide where in the triplet manifold these processes may be occurring, as only the lowest triplet state generally emits.[6,7]

If a second state, T_2, exists that can also be "over-populated" and have processes occurring from it (see Figure 1) then the decay problem becomes:

$$\frac{d[T_1]}{dt} = -(k_{10} + k_{12})[T_1] + k_{21}[T_2] \quad (3)$$

$$\frac{d[T_2]}{dt} = k_{12}[T_1] - (k_{20} + k_{21})[T_2] \quad (4)$$

where the rates are defined in Figure 1.

These coupled differential equations may be solved using LaPlace Transforms as by the method of DiBartolo.[8] While there is not much value in deriving the results, they are worth examining - especially in certain limits - as they illustrate what can be learned from a study of decay times.

Assuming processes linking levels 1 and 2 are faster than the other processes leaving T_1 and T_2 (i.e., k_{10} and k_{20}), then the general solution to equations (3) and (4) are:

$$[T_1] = \left[\frac{k_{21}([T_2]_0+[T_1]_0)}{k_{12} + k_{21}}\right]e^{-pt} + \left[\frac{k_{12}[T_1]_0-k_{21}[T_2]_0}{k_{12} + k_{21}}\right]e^{-qt} \quad (5)$$

Figure 1. Rate processes for a two level triplet system

$$k_{10} = k_{10}^{nr} + k_{10}^{r}$$

$$k'_{20} = k_{20}^{nr} + k_{20}^{r}$$

$$k_{20} = k'_{20} + k_{2p}$$

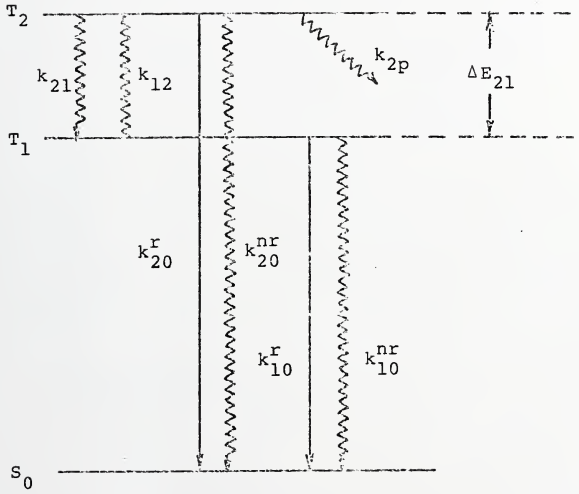
T_2
k_{21}
k_{12}
k_{2p}
ΔE_{21}
T_1
k^r_{20}
k^{nr}_{20}
k^r_{10}
k^{nr}_{10}
S_0

$$[T_2] = [\frac{k_{12}\{[T_1]_0+[T_2]_0)}{k_{12} + k_{21}}]e^{-pt} + [\frac{k_{12}[T_2]_0-k_{12}[T_1]_0}{k_{12} + k_{21}}]e^{-qt} \quad (6)$$

where $p = (\frac{k_{10}k_{21} + k_{12}k_{20}}{k_{12} + k_{21}})$

and $q = k_{12} + k_{21}$

Thus, the presence of a second level changes the decay of T_1 from exponential to nonexponential (where nonexponential means a sum of exponentials). Additional information can be gathered from these equations by considering two important cases of the general equations (3) and (4): thermal equilibrium and thermal activation (or deactivation).

Decay from Thermally Equilibrated States

If thermal equilibrium exists between T_1 and T_2 then:

$$\frac{[T_2]_0}{[T_1]_0} = \frac{k_{12}}{k_{21}} = e^{-\Delta E_{21}/kT} \quad (7)$$

where ΔE_{21} = energy separation between T_1 and T_2

k = Boltzmann's constant

T = temperature in K

and the general solutions given by equations (5) and (6) become:

$$[T_1] = (\frac{k_{21}}{k_{12} + k_{21}})([T_1]_0 + [T_2]_0)e^{-p't} \quad (8)$$

$$[T_2] = (\frac{k_{12}}{k_{12} + k_{21}})([T_1]_0 + [T_2]_0)e^{-p't} \quad (9)$$

where $p' = \frac{k_{10} + k_{20}e^{-\Delta E_{21}/kT}}{1 + e^{-\Delta E_{21}/kT}}$

With $\frac{\Delta E}{kT} >> 1$, then equations (8) and (9) further reduce to:

$$[T_1] = [T_1]_0 e^{-p''t} \quad (10)$$

$$[T_2] = [T_2]_0 e^{-p''t} \quad (11)$$

where $p'' = k_{10} + k_{20}e^{-\Delta E_{21}/kT}$

Thus, if a thermal equilibrium exists, the decay from either state will be exponential and show the same decay rate. Moreover, a study of the temperature dependence of the measured decays will give 1) the rates for leaving T_1 and T_2 for all processes except those linking these states, and 2) the energy separation between the levels. If more than two states are in thermal equilibrium then $k_{20}e^{-\Delta E_{21}/kT}$ is replaced by a sum of such terms as is the term $e^{-\Delta E_{21}/kT}$. If there are n levels in equilibrium then there will be n-1 such terms.

Decay with Thermal Activation (Deactivation)

If we consider where level 2 is thermally populated from level 1 but where $k_{21} = 0$, then the initial equations (3) and (4) may be solved exactly to give:

$$[T_1] = [T_1]_0 e^{-\beta t} \quad (12)$$

$$[T_2] = \{[T_2]_0 - \frac{k_{12}[T_1]_0}{-k_{10}-k_{12}+k_{20}}\}e^{-k_{20}t} + \frac{k_{12}}{k_{20}-k_{10}-k_{12}} e^{-\beta t} \quad (13)$$

where $\beta = k_{10} + k_{12}$

If k_{12} is an Arrhenius-type rate, i.e., $k_{12}=k_{12}^{\circ}e^{-\Delta E_{21}/kT}$, (where ΔE_{21} is not necessarily the difference in energy between the two levels) then equations (12) and (13) remain unchanged and β becomes

$$\beta = k_{10} + k_{12}^{\circ}e^{-\Delta E_{21}/kT}$$

Thus a nonexponential decay from only the upper state is predicted and at least one of the lifetimes from each state should show a temperature dependent behavior. The temperature dependent rate, which will be common to both states, can yield information on the rate of depopulation of T_1, on the energy barrier between states T_1 and T_2, and the intrinsic rate of conversion from T_1 to T_2. The other decay will give information (if seen) on the rate of depopulation of T_2.

If $k_{12} = 0$ instead of $k_{21} = 0$, then the roles of T_1 and T_2 are reversed (the actual equations may be obtained by changing subscripts 1 to a 2 and 2 to a 1 in equations (12) and (13)) and the decay from the lower state will be nonexponential. If both k_{12} and k_{21} are zero, then the two triplet levels are no longer coupled and the solutions are trivial:

$$[T_1] = [T_1]_0 e^{-k_{10}t} \tag{14}$$

$$[T_2] = [T_2]_0 e^{-k_{20}t} \tag{15}$$

Difficulties in the Interpretation of Phosphorescence Decays

There are many practical problems in the interpretation of the decay results from a lowest triplet state. The appearance of a nonexponential decay in itself does not prove that an upper triplet level is feeding a lower one since the existence of more than one emitting species caused by, say, environmental effects, tautomerization, etc.,

will also produce a nonexponential decay. On the other hand, a nonexponential decay caused by an upper triplet level may appear as an exponential decay if the intensity of one of the decays is sufficiently small or if one of the decays is sufficiently fast to avoid detection in a given experimental configuration.

Similarly, a change in the nonradiative decay rate as a function of temperature may be induced by, say, an upper reactive triplet state or by vibrationally induced intersystem crossing from T_1 to S_0. Fortunately, processes such as vibrationally activated intersystem crossing usually have much smaller preexponential factors and activation energies than such processes as reactions and hence can be distinguished by temperature dependent decay studies.[9]

Changes in steady state emission intensities may also be used to determine the values for such parameters as the energy separation between levels. Finally, it is important to remember that changes in steady state emission intensities may be effected by any process in the ground or first excited singlet state that will effect the number of molecules that intersystem cross to the triplet state.

Experimental Apparatus and Procedures

Phosphorescence Spectra

The apparatus for recording phosphorescence spectra is shown in Figure 2. The lamp source was either a 1000 watt d.c. Xenon arc lamp or a 12 watt low pressure mercury

Figure 2. Experimental configuration for recording spectra

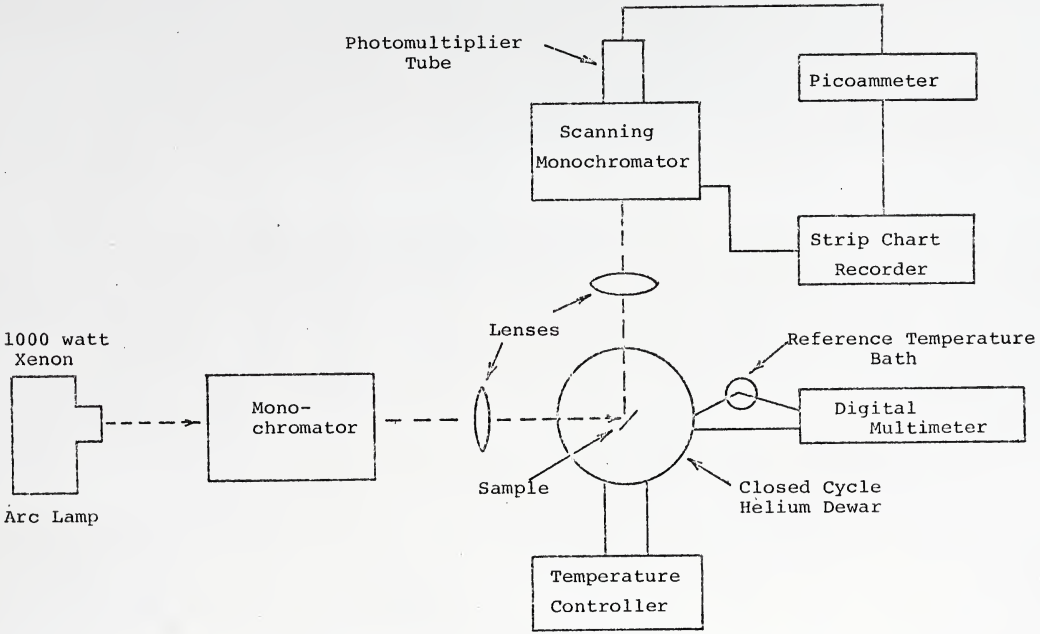
Photomultiplier Tube
Picoammeter
Scanning Monochromator
Strip Chart Recorder
Lenses
1000 watt Xenon
Reference Temperature Bath
Mono-chromator
Digital Multimeter
Sample
Closed Cycle Helium Dewar
Arc Lamp
Temperature Controller

vapor lamp. The excitation wavelength was selected by means of a 1/4 meter Scanning Monochromator (Heath Model 700) or an appropriate combination of filter solutions. This output was focused by means of Suprasil quartz lenses (Amersil, Inc.) onto a sample which was located at the tip of a closed cycle refrigerator (Air Products and Chemicals, Inc. Model CSW 202A Displex), range 10 to 300K.

The sample holders were of homemade design and were constructed from oxygen-free copper to insure high thermal conductivity. Temperatures were monitored via a pair of Chromel P vs. Gold,/.07 atomic % Iron thermocouples. One was located in the tip of the Displex and used as input for an Indicating Temperature Controller (Air Products and Chemicals, Inc. Model APD-IC 1) that had a ± 1K temperature control for a 48 hour period. The other thermocouple was held in place by a set screw at the bottom of the sample holder and used a liquid nitrogen bath as a reference. The output of this thermocouple was monitored on a Digital Multimeter (Keithley Model 160) whose readings were converted to degrees K with an accuracy of ± 0.1K. The two thermocouples always agreed to within the reading errors of the monitoring instruments but the second thermocouple because of its smaller reading error and position was taken as more accurate.

Sample emission was collected at right angles to the excitation beam and focused by means of Suprasil quartz lenses onto the slits of a second 1/4 meter Scanning Mono-

chromator (Heath Model 700) which had a photomultiplier tube (EMI 9558Q or EMI 9635 QB) with quartz window at its exit slit. The signal from this tube was filtered and amplified by a Picoammeter (Keithley Model 416) and recorded on a Strip Chart Recorder (Heath Model EU-205-11) synchronized to the second monochromator drive.

Phosphorescence Lifetimes

The apparatus for measuring the lifetimes is shown in Figure 3. The same excitation lamps were used as before, but since the intensity of exciting light was more important than its monochromaticity for the lifetime work, optical cells were used instead of the monochromator for isolating the excitation wavelength. Actually, for the work involving the low pressure mercury vapor lamp, even the optical cells were omitted if there was no mercury line near the band whose lifetime was being measured. Prior to impinging on the sample the excitation light was chopped by means of a mechanical chopper whose speed was controlled by a variable frequency oscillator. The sample holders and temperature control systems were as previously described as were the focusing optics, analyzing monochromator and photomultiplier tube.

The output of the photomultiplier tube was directed to the input of a Digital Signal Averager (Tractor - Northern Scientific, Inc. Model NS-570). The instrument's input resistance is one megaohm; since its Analog-to-Digital Converter requires only 100 millivolts for a full scale reading,

Figure 3. Experimental configuration for recording lifetimes

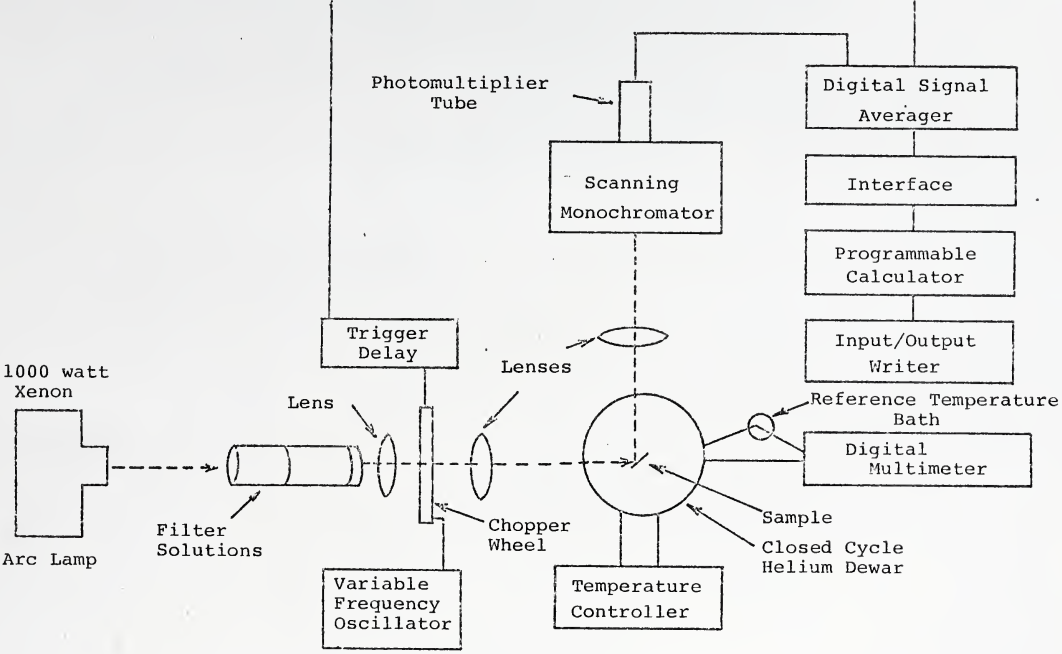
Photomultiplier Tube
Digital Signal Averager
Scanning Monochromator
Interface
Programmable Calculator
Input/Output Writer
Trigger Delay
Lenses
1000 watt Xenon
Lens
Reference Temperature Bath
Digital Multimeter
Filter Solutions
Chopper Wheel
Sample
Closed Cycle Helium Dewar
Arc Lamp
Variable Frequency Oscillator
Temperature Controller

a 100 nanoamp current is required to provide this reading. In practice, only 20-30 nanoamps are drawn from the photomultiplier tube, a value well below saturation current level.

The signal averager contains 1024 channels. The decay signals were allowed to build up until a good signal-to-noise ratio was obtained. The capacitance of the system, as determined by the photomultiplier tube, interconnecting cable and a variable filter placed across the input resistor of the signal averager - was adjusted such that the RC time constant of the system was less than the sweep time for a single channel.

The signal averager was triggered off the chopper system using a delayed triggering scheme that eliminates any contribution to the decay signal from the mechanical chopper. The amount of decay time required for any given chopper frequency is determined by noting the effect of excitation light on the signal averager and simply delaying the sweep until this light produces no effect in the signal averager.

The output of the signal averager is dumped via an interface (Wang Model 705-1A Microface) into a Programmable Calculator (Wang Model 700C) that analyzes the decay curve. Exponential curves are most conveniently handled, but the system has the capacity to handle dual exponential curves also. The basic program used in the analysis was written by Dennis Mahoney,[10] although a few alterations were necessary

because of the use of a different signal averager in our work. The program deconvolutes nonexponential decays by first calculating the lifetime result for the long-lived emission starting from a time when the short-lived emission has essentially ceased. It then subtracts off the contribution of the long-lived emission from the actual emission and calculates a lifetime for the short-lived emission. Choice of the point where the short-lived emission ceases to influence the results is chosen by the operator from a plot of ln Intensity (actually ln of the number of counts) versus time that is printed out on an Input/Output Writer (Wang Model 711). For good input data, the lifetime results should be accurate to about 10%, if the lifetimes are different by at least a factor of two and the decays are roughly of the same initial intensity. Lifetimes are calculated using a weighted least squares procedure that weights each point as the square of the signal intensity. Thus, points where the signal-to-noise ratio is high are more highly weighted.

CHAPTER II
BEHAVIOR OF TRIPLET BENZENE

Introduction

Benzene Phosphorescence

Lewis and Kasha[3] measured the phosphorescence spectrum of benzene in EPA (5:5:2-ether, isopentane, alcohol by volume) and noted its very high triplet energy (about 85 Kcal) and its relatively broad though somewhat structured appearance. Shull[11] reinvestigated the same system and from a detailed vibrational analysis concluded that the symmetry of the emitting state was B_{1u} and the geometry was hexagonally symmetric planar. Later work by Albrecht[12] confirmed this symmetry assignment and elucidated the pathways of vibronic spin-orbit coupling. Nieman and Tinti[13] and de Groot and van der Waals[14] further showed that Shull's deduction of hexagonal symmetry was in error and that in fact the triplet state geometry is planar elongated (D_{2h}).

Lewis and Kasha had not attempted to measure the benzene phosphorescence lifetime, but later workers have done so despite the early instrumental difficulties caused primarily by the very weak emission intensity. In 1949, McClure[15] reported that triplet benzene had a lifetime of 7.0 ± 0.5 seconds in EPA at 77K. Coupled with later quantum yield work, he deduced a value of 21 seconds for the radiative lifetime of benzene. This value was later corrected by

Lim[17] to 28 ± 2 seconds.

Even with the advent of more sophisticated instrumentation, differences in the values for the benzene phosphorescence lifetime were reported varying from solvent to solvent and, in some instances, even in the same solvent. Working at 4.2K, Wright, Frosch, and Robinson[18] recorded benzene lifetimes of 16 seconds (in methane and in argon) and benzene-d_6 lifetimes of 22 seconds (methane) and 26 seconds (argon). Russell and Albrecht[19] reported that benzene has a triplet lifetime of 5.2 seconds in 3MP (3-methylpentane) at 77K. Martin and Kalantar[20] reported a slight deviation from exponential decay for benzene in either EPA or 3MP at 77K and state that the measured lifetime in these solvents varies with the cooling time of the sample. Benzene lifetimes in EPA varied from 7.80 to 8.45 seconds over a five-hour period while in 3MP the lifetimes varied from 4.70 to 5.75 seconds over a three hour period.

Temperature-Dependent Work

The temperature dependence of benzene's phosphorescence lifetime was studied by three separate groups: Nieman, Hatch, and Erlitz,[21] Leubner and Hodgkins,[22,23] and Kilmer and Spangler.[24] Their results showed a remarkable dependence of benzene lifetime on both solvent and temperature. For any given solvent the lifetimes were usually temperature independent below 50 - 60K, but varied rapidly above this onset temperature. This resolved the problem of the lifetime variation in the same solvent (i.e., the temperatures were

not identical) and focused attention on the probable causes of this effect.

Nieman et al. found that the temperature-dependent results could be fit to an equation of the form:

$$k_{obs} = k_{LT} + Ce^{-\Delta E/kT} \quad (16)$$

where k_{obs} = observed decay rate

k_{LT} = low temperature decay rate

C = constant

ΔE = activation energy

T = temperature in K

k = Boltzmann's constant

Furthermore, k_{LT}, C and ΔE were found to vary in an apparently arbitrary manner with solvent. C was found to vary between 10^{+3} and 10^{+9} with ΔE of the order of 500 - 2000 cm^{-1}.

At this time several investigators[9,25-30] reported quantum theories for the radiationless transitions in large molecules and two in particular looked specifically at the temperature dependence of benzene phosphorescence. Fischer[29] attributed the strong temperature dependence to the pseudo-rotational motion of benzene in the lowered D_{2h} symmetry of the triplet state. This approach has been criticized[31,32] on several grounds. First, this equation does not give a good fit to the experimental results throughout the temperature range investigated.[31] Second, and more importantly, pseudorotation and temperature-dependent lifetimes do not always occur in the same temperature region. The phosphorescent lifetime work of Nieman et al.[32] for mesitylene

in B-trimethylborazine show a temperature-dependent lifetime above 150K while the ESR work of van der Waals[33] indicates that the mesitylene is freely interconverting among its various forms by 77K.

Lin[9] has derived a theoretical expression for the temperature dependence which is identical in form to the empirical one of Nieman, et al., but his estimates of the intramolecular radiationless decay rates (C) are orders of magnitude too small. Despite a great deal of discussion, there appears to be no generally accepted explanation for the strong temperature dependence of benzene's phosphorescence and for its strong solvent dependence, although several have been proposed. Since the ΔE values are of the same order of magnitude as vibrational energies, vibrations of either the benzene[21,23] or of the solvent[23] have been cited for the effect. At high temperatures in electronically excited benzene, different isomeric forms of benzene (that revert to ordinary benzene in the ground state) have been found,[34,35] and have been proposed as the cause of the effect. Currently, there is no conclusive explanation of the observations.

Benzene Photochemistry

In 1953, Gibson, Blake, and Kalm[36] discovered that benzene when irradiated in IM (isopentane, methylcyclohexane) or EPA at 77K produced a photoproduct that had a spectrum similar to that of hexatriene. Subsequent independent work by Leach and Migirdicyan[37-42] and by Anderson, Chilton, and Porter[43] showed that the photoproduct formed was a solvent substituted

hexatriene. Leach and Migirdicyan proposed that the reaction went by a biradical mechanism,[37,39,42] while Porter et al. proposed a four-center concerted mechanism.[43] Subsequent ESR work[44] failed to provide any evidence for the hexatriene biradical and thus a concerted mechanism is assumed operative. Photoproduct formation is found to depend linearly on exciting light intensity;[45] of the two possible precursor states (i.e., the first excited singlet state or the triplet state), the longer lifetime of the triplet is thought to make it the more likely precursor.

In 1962, Shelimov, Fok, and Voevodskii[46] reported that while irradiating benzene with 254 nm light in a solvent glass at 77K, solvent radicals were produced. In 3MP, the radical was formed by breakage of the C-H bond of the tertiary carbon atom. It was later found that this process required the absorption of two photons[47] and as the excited singlet state is too short-lived for this to occur, an upper triplet is assumed responsible for the radical formation.[47,48] Using this fact and making certain assumptions about the radical-forming process, they were able to obtain a spectrum of the excited triplet level by following radical production as a function of the wavelength of exciting light from a second light source.[49] The second triplet of benzene lies approximately 1 eV above the first.

Benzene-Polyhaloalkane Complexes

In 1969, Simons and Perrins[50] reported their results for the system: benzene (10^{-3} M), chloroform (10^{-1} M), IM

(isopentane, methylclcohexane) solvent at liquid nitrogen temperatures. Chloroform has long been known[51] to possess an affinity for benzene at room temperature and Simons et al. were able to show that a 1:1 complex of chloroform with (ground state) benzene was formed at lower temperatures with a ΔH_f of -1170 ± 120 cal/Mole and a ΔG of -354 ± 70 cal/Mole. The complex persisted in the first excited singlet state of benzene with a ΔH_f of -590 ± 180 cal/Mole. A 2:1 chloroform-benzene complex was also found at higher relative chloroform concentrations.

Analyzing the phosphorescence spectrum in 3MP, Simons, Perrins, and Smith[52] discovered that there was a substantial change in its appearance and that the spectrum was consistent with a D_{2h} symmetry for the benzene. It was noted that compounds like C_2HCl_5 had a similar effect to chloroform, but that chlorocarbons like CCl_4 showed no evidence of complexation whatsoever.[50] They further found that with the chloroform present the photoproduct changed from a solvent-substituted hexatriene to a chloroform-substituted hexatriene.[50] A change from chloroform to chloroform-d as the complexing agent produced no change in the spectroscopic results for the ground and first excited singlet levels, but resulted in the solvent-substituted hexatriene being formed as the photoproduct although this occurred at a slower rate than in the absence of the chloroform-d.[50] From phosphorescent lifetime work at 77K, Simons and Smith[53] established that changes in the lifetime accompanied this change in photo-

product formation and they also noted a puzzling nonexponential decay from the benzene-chloroform complex while the benzene-chloroform-d complex decayed exponentially.

Later work[54] on hexatriene formation from benzene derivatives (substituted as highly as hexaethylbenzene) led them to conclude that steric factors were important in hexatriene formation. They concluded that the chloroform sits with the C-H bond of the chloroform on the six-fold axis of the benzene and that a tilt of the chloroform must occur to achieve hexatriene formation. Similar work on benzene in either ethanol, ethanol-d, or ethanol-d_6[55] led them to conclude that an intermolecular vibronic coupling is operative in these systems and is instrumental in the radiationless decay of the triplet state.

Benzene Dissertation Work

In the first part of this dissertation, the phosphorescence decay times of the benzene:chloroform:alkane system have been investigated as a function of temperature. The results have been fit to a rate equation of the form used by Nieman and the parameters thus obtained used to elucidate the radiationless processes in benzene. The nonexponential decay exhibited by the chloroform-benzene system has also been studied and related to data already available.

To account for the data we propose that an exciplex is formed between triplet benzene, chloroform, and the solvent. This model also provides a framework for understanding a wide variety of photochemistry involving benzene in differ-

ent phases. Calculations have been performed using open and closed shell Intermediate Neglect of Differential Overlap (INDO) semi-empirical theories that show the validity of our arguments and shed additional light on the structure of the hexatriene precursor.

Experimental Procedures

Table I is a list of chemicals used, along with their source and purity. Each solvent was irradiated with 254 nm light in order to show that there was no impurity emission that would interfere with the (0,0) emission (~338-340 nm) of the benzene-chloroform complex. This is the spectral region of importance in this experiment as benzene itself has essentially no (0,0) emission and hence uncomplexed benzene cannot interfere with either the spectral or lifetime results of the complex in this region.

Each solvent was passed through a gas chromatograph in order to identify any significant impurity that could complex with the benzene. Chloroform was found to contain some traces of acetone, but acetone was not found to complex with benzene. We also checked on the possibility of toluene affecting the results, but found that the complex formed with chloroform emits some 6 nm to the red of the benzene-chloroform complex and hence could not have significantly affected the results, even if it had been there in appreciable concentrations.

Spectra were recorded using the low pressure mercury

Table I
Chemicals, Their Source and Purity

Chemical	Source	Grade or Purity
Benzene	Matheson, Coleman & Bell Norwood, Ohio	Spectrograde
Benzene-d_6	Aldrich Chemical Co., Inc. Milwaukee, Wisconsin	99.5 atom %
Chloroform	Malinckrodt St. Louis, Missouri	Spectrograde
Chloroform-d	Aldrich Chemical Co., Inc. Milwaukee, Wisconsin	99.8 atom %
3-Methylpentane	Aldrich Chemical Co., Inc. Milwaukee, Wisconsin	99+ %

vapor lamp since its output in the 254 nm region is more than ten times that of the xenon arc lamp. Filter solutions in the excitation pathway were used if a spectrum of the entire emission region was required. In general, only the (0,0) band was monitored; since the lamp had no significant emission in this region, spectra were frequently recorded without even the use of filter solutions. The slit widths for these runs were generally on the order of 150 microns (band pass: 0.3 nm).

For the lifetime work, the mercury vapor lamp without cells was used. Slits were typically between 900 and 1200 microns for a band pass of 1.8 to 2.4 nm. Decay curves were recorded over a period of four lifetimes. If decay curves were nonexponential, then they were recorded for four lifetimes of the longer lived species.

The design for the sample holder used in this work is shown in Figure 4. Light could enter the cell through the small window A and emission could be viewed at right angles to the excitation source through window B. Alternatively, the cell could be placed at 45° to the excitation beam and then both exciting and emitted light would pass through window B. The former arrangement has the advantage of effectively screening the analyzing equipment from the excitation beam, while it suffers from the disadvantage of screening the analyzing equipment from emission that occurs near the surface of window A. As benzene is a strong absorber of 254 nm light, much of the emission would be lost if the sample were excited through

Figure 4. Sample holder

A Window A for excitation light

B Window B for excitation and/or emitting light

C Cover plate to hold windows

D Threaded screw for mounting on Displex

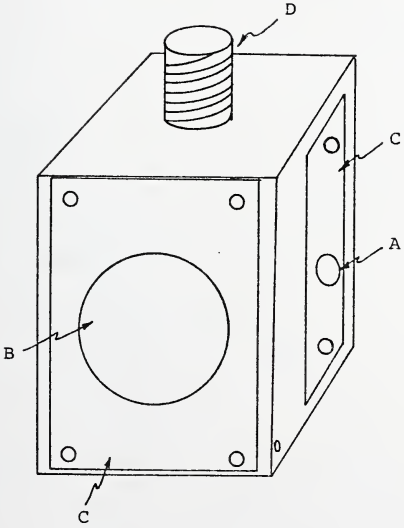
D
C
A
B
C

window A and hence the latter configuration was used almost exclusively. As liquids may readily lose 1/4 to 1/2 their volume on cooling, a metal plate in the shape of a semi-circle was frequently placed at the bottom of the cell holder to increase the height of the glass layer that is close to window B. Thus, the top half of the sample holder served as a reservoir of solution for the glass forming process. The O-ring seal in the sample holder prevented the liquid from being exposed to vacuum during the cooling process. In practice, very little, if any, solution was found to be lost during the run. This design, however, prevented the solutions from being degassed. Dry nitrogen was bubbled through the solutions to remove oxygen which is frequently[6] (although not usually for benzene)[24,56] a triplet quencher. The sample cell was filled in a nitrogen atmosphere.

The solutions were prepared by placing 3.5 µl of benzene (from a 10 µl syringe) and 320 µl of chloroform (or chloroform-d) into a 10 ml volumetric flask and filling to volume with 3-methylpentane (3MP). This makes a solution of 3.94 mM benzene and .399 M chloroform (.399 M chloroform-d). Solutions with one tenth of the above chloroform concentration were also prepared in order to study the effect of concentration on the spectrum.

Samples were cooled directly from room temperature to operating conditions (10 to 90K) on the Displex. Stopping the cooling process of the solution at the freezing point of the glass and waiting 30 minutes was found to not

significantly affect the results. Two hours were allowed for thermal equilibrium to be attained in the glass. Any temperature changes required during the experiments were kept to less than 10K and a period of 30 minutes was allowed for thermal equilibrium to be reestablished. It is important to observe that our method of sample preparation, while corresponding to a slow cooling process (3K per minute) probably results in a nonequilibrium ratio of free benzene to 1:1 to 2:1 (chloroform to benzene) complex by freezing some higher temperature configuration in the glass.

Experimental Results

Spectral Results

The spectra of benzene and its complexes with chloroform and chloroform-d at approximately 15 and 77K in 3MP are shown in Figures 5 and 6. The spectra at 77K have been reported previously[19,52] and our spectra essentially agree with these results. There is some change in the spectra upon further cooling, with some peaks showing a doublet character at the lower temperature. The benzene spectrum shows almost no emission in the 338-340 nm region where its 0,0 band is located, but does show 992 cm^{-1} ring breathing mode progressions based on false origins corresponding to one quanta of the ν_8 mode (1596 cm^{-1}; symmetry e_{2g}) and one quanta of the ν_9 mode (1178 cm^{-1}; symmetry e_{2g}). The benzene-chloroform spectra show an intense 0,0 transition on which are built progressions in the 992 cm^{-1} mode. Similar progressions

Figure 5. Phosphorescence spectra of benzene and its complexes at 15K

Top - C_6H_6-$CHCl_3$

Middle - C_6H_6

Bottom - C_6H_6-$CDCl_3$

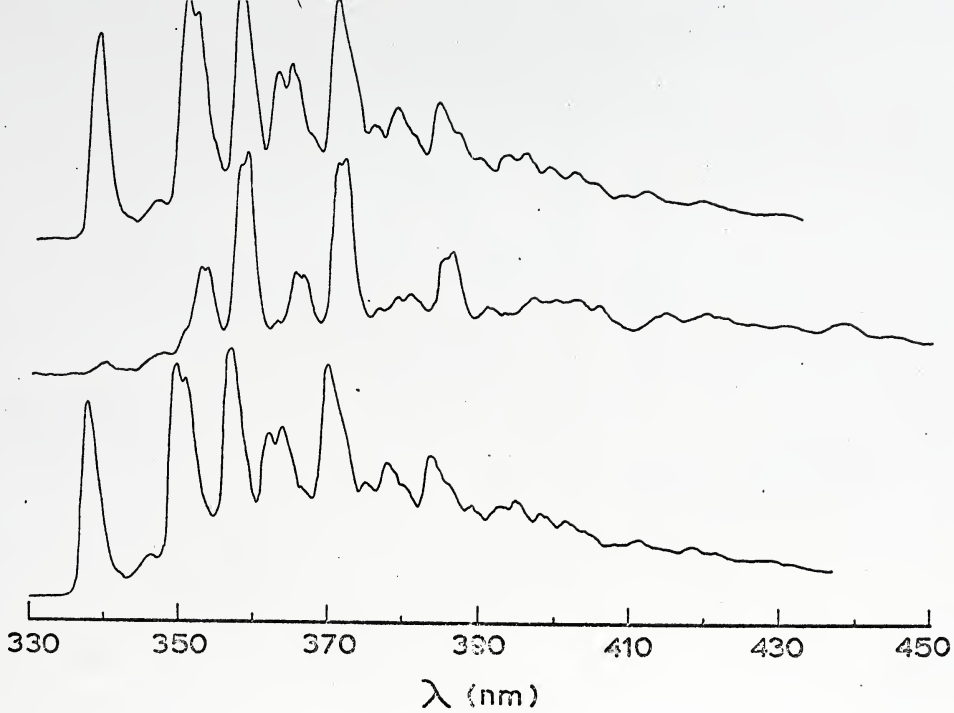
330
350
370
390
410
430
450
λ (nm)

Figure 6. Phosphorescence spectra of benzene and its complexes at 77K

Top - C_6H_6-$CHCl_3$

Middle - C_6H_6

Bottom - C_6H_6-$CDCl_3$

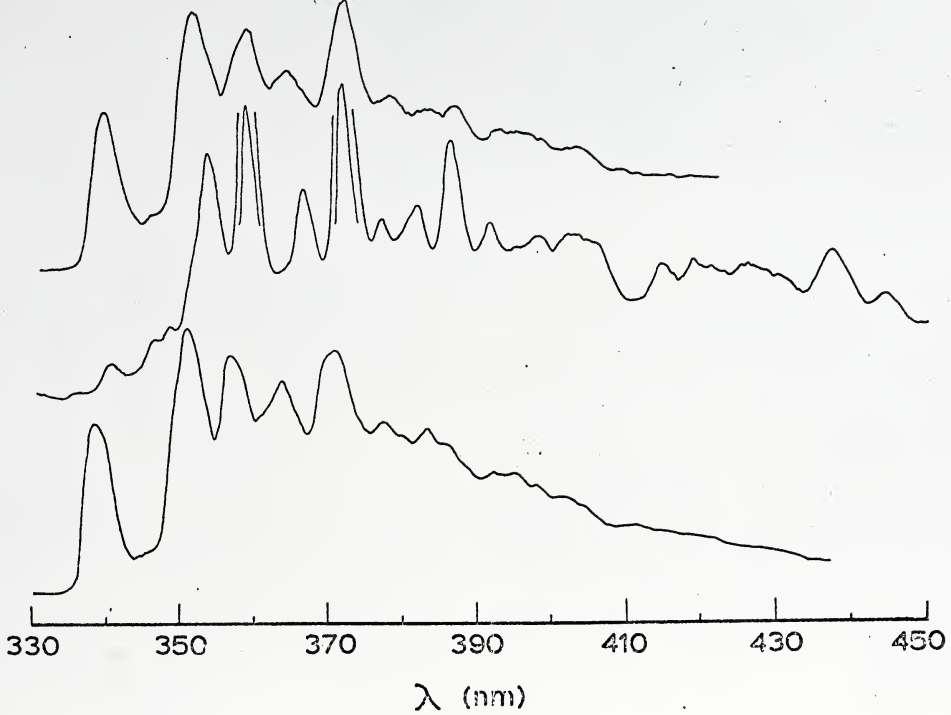
330
350
370
390
410
430
450
λ (nm)

built on the false origins corresponding to one quantum of the ν_8 and ν_9 modes are also observed.

Figure 7 is a plot of the natural logarithm of the intensity of the origin emission (0,0 band for the complexes or false origin for the benzene) versus temperature and show the strong dependence of emission intensity on temperature. Figure 8 shows the effect of "slow" cooling (stopping for 1/2 hour at the freezing point of the glass) on sample emission intensity. In spite of an apparent effect on the temperature dependence of the emission intensity, there was no apparent difference in the emission spectra for the complex formed by the different procedures.

Lifetime Results

Working solely in the 338-340 nm region, decay curves for emission from the complexes were obtained. From a plot of ln (Intensity) versus time (see Figure 9) it is easily seen that these curves are nonexponential. These curves were deconvoluted by the method previously described. The results for each component lifetime of each complex as a function of temperature (13-90K) are shown in Figures 10 and 11. Figures 12 and 13 are plots of the decay rate versus the inverse of the temperature for the same results. Above 80-90K, the intensity of the 0,0 band is too small to allow the measurement of lifetimes on our equipment.

In Tables 2 and 3, the results for various fitting schemes for the data are given. In each case a weighted least squares program identified as Super, provided and

Figure 7. Plot ln (I/I_0) versus temperature for complexe and uncomplexed benzene

I = Intensity at temperature T

I_0 = Intensity at lowest temperature

□ = C_6H_6

Δ = $CDCl_3$-C_6H_6

⊙ = $CHCl_3$-C_6H_6

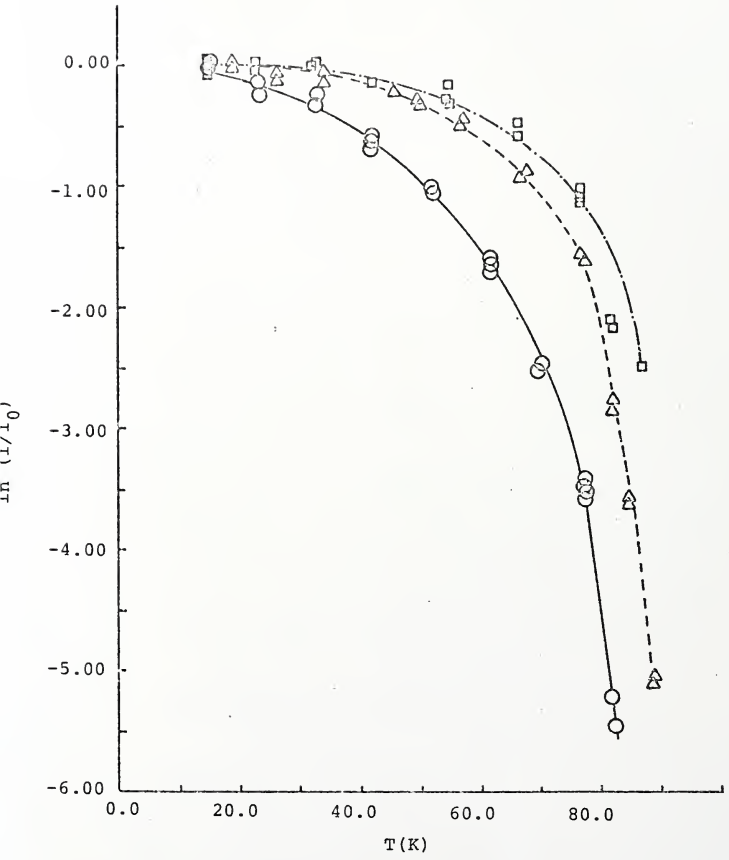
0.00
-1.00
-2.00
-3.00
-4.00
-5.00
-6.00
0.0
20.0
40.0
60.0
80.0
T(K)
ln (I/I0)

Figure 8. Plot ln (I/I_0) versus temperature for slow and normal cooled complexed benzene

I = Intensity at temperature T

I_0 = Intensity at lowest temperature

⊙ = $CHCl_3$-C_6H_6: normal cooling

Δ = $CHCl_3$-C_6H_6: slow cooling

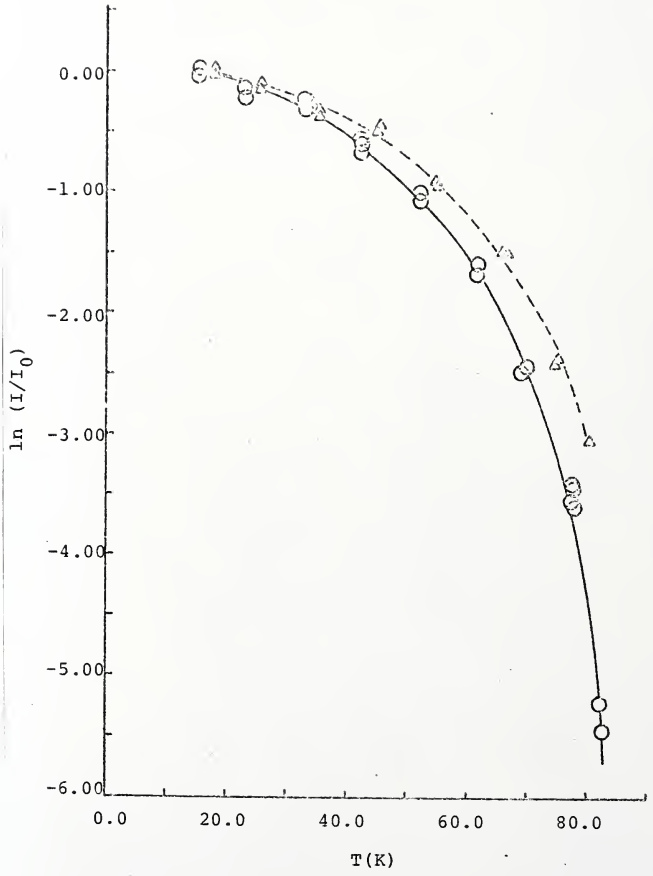
0.00
-1.00
-2.00
-3.00
-4.00
-5.00
-6.00
ln (I/I0)
0.0
20.0
40.0
60.0
80.0
T(K)

Figure 9. Plot of ln (relative intensity) versus time for a typical run

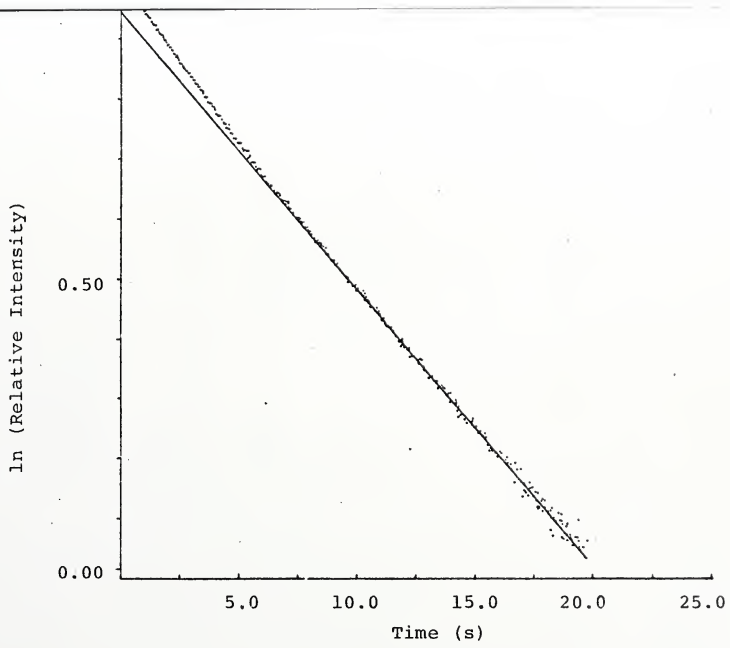
ln (Relative Intensity)
0.50
0.00
5.0
10.0
15.0
20.0
25.0
Time (s)

Figure 10. Plot of lifetime versus temperature for the benzene-chloroform complex

O = Long-lived component

Δ = Short-lived component

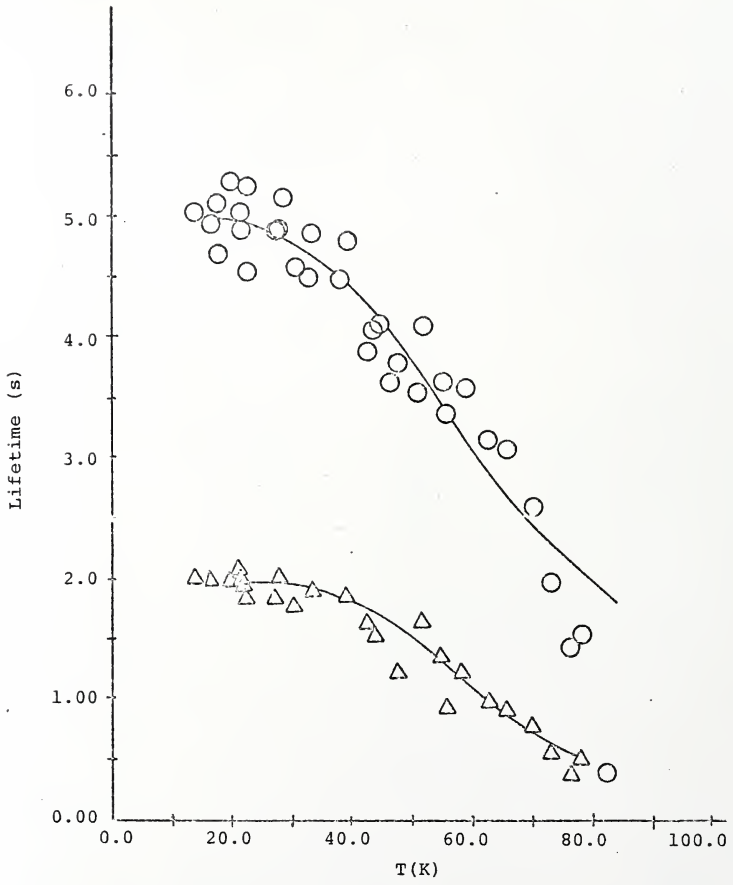
6.0
5.0
4.0
3.0
2.0
1.00
0.00
Lifetime (s)
0.0
20.0
40.0
60.0
80.0
100.0
T(K)

Figure 11. Plot of lifetime versus temperature for the benzene-chloroform-d complex

O = Long-lived component

Δ = Short-lived component

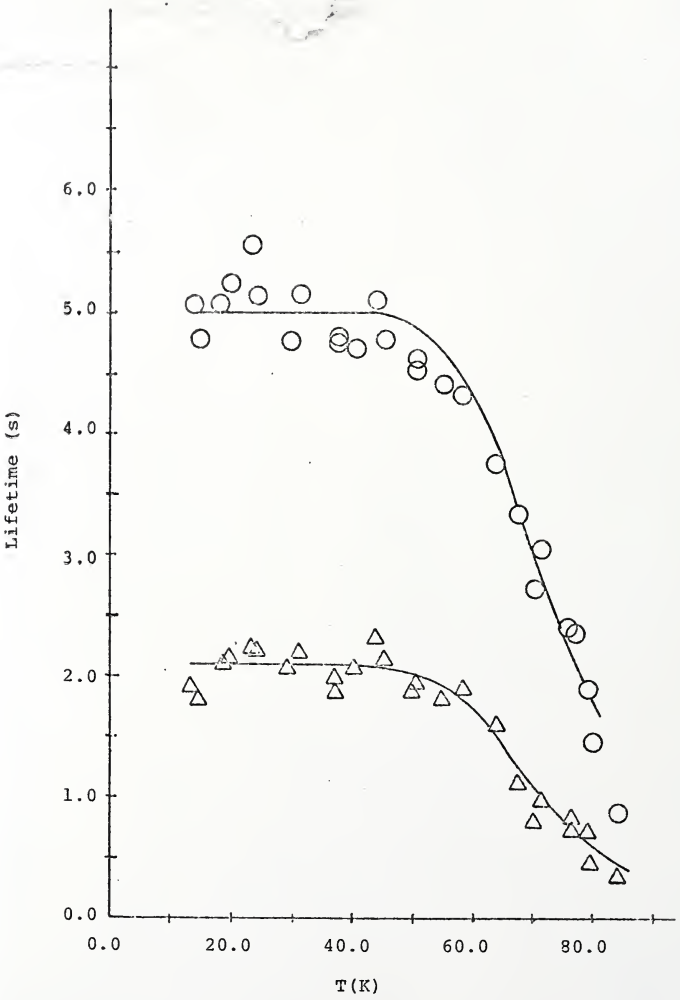
Lifetime (s)
6.0
5.0
4.0
3.0
2.0
1.0
0.0
0.0
20.0
40.0
60.0
80.0
T(K)

Figure 12. Plot of decay rate versus inverse temperature for the benzene-chloroform complex

O = Long-lived component

Δ = Short-lived component

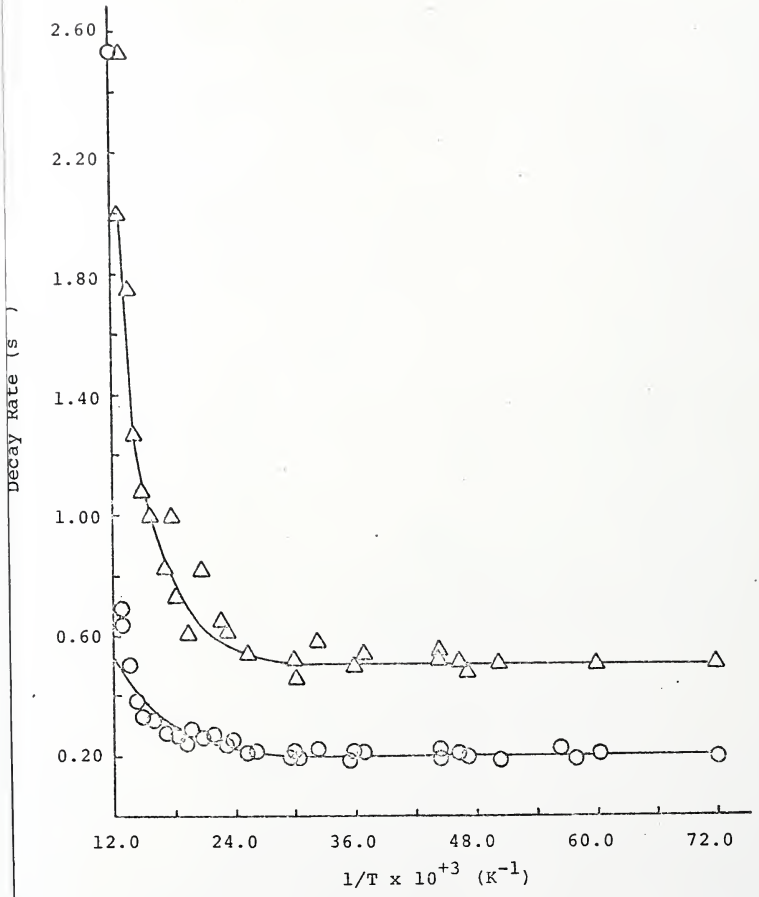
2.60
2.20
1.80
1.40
1.00
0.60
0.20
Decay Rate (s⁻¹)
12.0
24.0
36.0
48.0
60.0
72.0
1/T x 10+3 (K-1)

Figure 13. Plot of decay rate versus inverse temperature for the benzene-chloroform-d complex

O = Long-lived component

Δ = Short-lived component

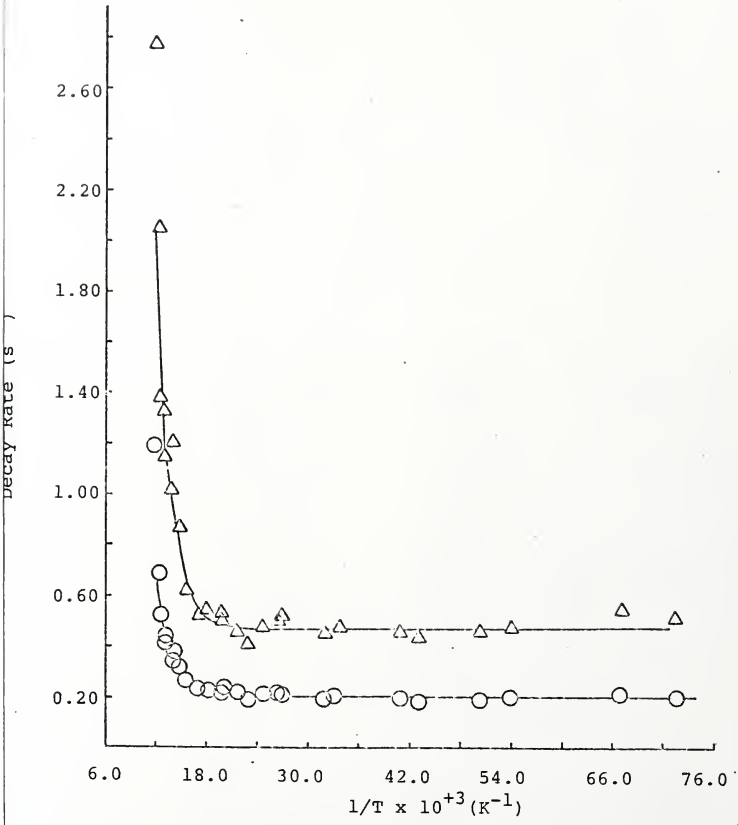
2.60
2.20
1.80
1.40
1.00
0.60
0.20
6.0
18.0
30.0
42.0
54.0
66.0
76.0
1/T x 10+3 (K-1)

Table 2
Parameters Determined from Observed Decay Rates for Benzene Complexes
(Forms I and II)

		Slow Decay Rate			Fast Decay Rate		
Complex	Form	$k_{10}(s^{-1})$	$k_{20}(s^{-1})$	$\Delta E_{21}(cm^{-1})$	$k_{10}(s^{-1})$	$k_{20}(s^{-1})$	$\Delta E_{21}(cm^{-1})$
C_6H_6-$CHCl_3$	I	.205±.005	5.4±2.6	160±20	.52±.02	130±70	240±30
C_6H_6-$CHCl_3$	II	.205±.005	6.4±3.0	160±20	.52±.02	130±70	240±30
C_6H_6-$CDCl_3$	I	.203±.004	660±650	420±50	.48±.01	2200±3000	420±70
C_6H_6-$CDCl_3$	II	.203±.004	660±650	420±50	.48±.01	2200±3000	420±70

Form I $$k_{obs} = k_{10} + k_{20}e^{-\Delta E_{21}/kT}$$

Form II $$k_{obs} = \frac{k_{10} + k_{20}e^{-\Delta E_{21}/kT}}{1 + e^{-\Delta E_{21}/kT}}$$

k_{obs} = observed decay rate

Table 3
Parameters Determined from Observed Decay Rates for Benzene Complexes
(Forms III and IV)

		Slow Decay Rate			Fast Decay Rate		
Complex	Form	$C_{10}(s^{-1})$	$k_{20}(s^{-1})$	$\Delta E_{21}(cm^{-1})$	$C_{10}(s^{-1})$	$k_{20}(s^{-1})$	$\Delta E_{21}(cm^{-1})$
C_6H_6-$CHCl_3$	III	.2010	4.2±1.6	150±20	.5014	90±40	220±20
C_6H_6-$CHCl_3$	IV	.2010	5.0±1.8	150±20	.5014	100±50	220±20
C_6H_6-$CDCl_3$	III	.2000	450±400	400±50	.4736	1600±1900	400±60
C_6H_6-$CDCl_3$	IV	.2000	450±400	400±50	.4736	1600±1900	400±60

Form III $$k_{obs} = C_{10} + k_{20}e^{-\Delta E_{21}/kT}$$

Form IV $$k_{obs} = \frac{C_{10} + k_{20}e^{-\Delta E_{21}/kT}}{1 + e^{-\Delta E_{21}/kT}}$$

k_{obs} = observed decay rate

C_{10} = low temperature rate

modified by Joseph Baiardo,[57] was used to fit the results. The first form (I) is the one used originally by Nieman (see equation 16) while form II is the theoretical expression derived in the introduction (see equation 9). The third form is a modification of the first in which the low temperature decay rate, k_{10}, first found by averaging the low temperature results, is treated as a constant in the subsequent determination of k_{20} and ΔE_{21}. This form was explored because the data invariably showed a tendency to depart from I in the region where the decay rates first start to change. This deviation causes most fitting procedures to give a somewhat high value for k_{10} and correspondingly low values of k_{20} and ΔE_{21}.[21] This general result is not as pronounced here as in previous work because of the large decay rate errors caused by the nonexponential deconvoluting procedure. Form IV is the analogous modification of form II. The solid line in Figures 10 through 13 is the calculated fit to the data using form IV.

Tables 2 and 3 indicate that the accuracy of the k_{10} results are better than the 10% previously estimated, but this is felt to merely reflect a consistency in the choice of break point in the deconvolution procedure that does not necessarily denote accuracy. Table 4 gives the output of Super for form I using the data of the benzene-chloroform-d complex for both the slow and fast decay rates.

Table 4
Sample Fit to C_6H_6-$CDCl_3$ Decay Rates (Form I)

Temperature (K)	Experimental Rate (s^{-1})	Calculated Rate (s^{-1})	Percentage Deviation
		Fast Decay	
13.6	0.519	0.483	-7.0
14.9	0.552	0.483	-12.5
18.4	0.471	0.483	2.5
19.8	0.459	0.483	5.2
23.2	0.443	0.483	9.1
24.4	0.446	0.483	8.2
29.5	0.481	0.483	0.5
31.2	0.454	0.483	6.4
37.2	0.528	0.483	-8.5
37.4	0.506	0.483	-4.4
40.4	0.481	0.484	0.5
43.9	0.432	0.485	12.2
45.3	0.463	0.486	5.1
50.2	0.532	0.495	-7.0
50.5	0.511	0.496	-2.9
54.9	0.547	0.518	-5.3
58.3	0.529	0.550	4.0
63.5	0.618	0.640	3.5
67.6	0.875	0.763	-12.8
70.6	1.21	0.893	-25.9
71.6	1.01	0.945	-6.6
75.9	1.33	1.23	-7.8
76.9	1.15	1.31	14.1
79.3	1.39	1.54	10.7
79.8	2.06	1.59	-22.9
84.1	2.78	2.11	-24.0
		Slow Decay	
13.6	0.197	0.203	3.0
14.9	0.208	0.203	-2.1
18.4	0.196	0.203	3.8

Table 4 - continued

Temperature (K)	Experimental Rate (s^{-1})	Calculated Rate (s^{-1})	Percentage Deviation
19.8	0.190	0.203	7.2
23.2	0.181	0.203	12.2
24.4	0.194	0.203	4.6
29.5	0.210	0.203	-3.3
31.2	0.193	0.203	5.4
37.2	0.212	0.203	-4.0
37.4	0.209	0.203	-2.6
40.4	0.212	0.204	-3.8
43.9	0.195	0.204	4.4
45.3	0.210	0.204	-2.4
50.2	0.216	0.208	-3.8
50.5	0.221	0.208	-6.0
54.9	0.225	0.215	-4.5
58.3	0.230	0.226	-1.8
63.5	0.266	0.256	-3.8
67.6	0.299	0.297	-0.6
70.6	0.368	0.340	-7.6
71.6	0.327	0.357	9.3
75.9	0.415	0.450	8.4
76.9	0.421	0.477	13.1
79.3	0.518	0.549	6.0
79.8	0.686	0.566	-17.6
84.1	1.19	0.735	-38.2

Discussion

Spectral Results

Previous analysis of the uncomplexed benzene spectrum has indicated - on the basis of the absence of the 0,0 transition and presence of progressions based on false origins - that triplet benzene is only slightly distorted from D_{6h} symmetry.[13,14] Simons has shown that the symmetry of benzene in a complex is lowered to D_{2h}.[52] From this symmetry assignment and the relative vibrational intensities in the phosphorescence spectrum of the chloroform complex it has been shown[52,58] that the deviation from D_{6h} symmetry is at least three times that in the uncomplexed benzene.

Our phosphorescence spectral results show an apparent discrepancy with the benzene complex spectra of Simons. Relative to his results, our spectra show several peaks at higher energies. Simons has attributed several shoulders on the blue edge of his peaks to a 2:1 complex,[52] and we agree with this assignment. As previously mentioned, our experimental conditions probably cause a nonequilibrium ratio of 2:1 versus 1:1 chloroform-benzene complex pairs. With a slower cooling procedure it is expected that greater relaxation can occur and a different proportion of the chloroform-benzene complexes form. The slightly different temperature dependence for the benzene-chloroform complex phosphorescence intensities for the different cooling procedures (see Figure 8) are no doubt caused by this effect.

Strong support for the existence of two emitting species

comes from the shift in wavelength with temperature of the 0,0 band of the benzene-chloroform-d complex (see Figure 14). This shift can best be understood in terms of different intensity contributions from the two different complexes at different temperatures. Reduction of the chloroform concentration by a factor of ten also appeared to cause some shift in the location of the 0,0 band but this result is complicated by a lowering of the 0,0 band intensity and the appearance of new peaks that indicate the presence of uncomplexed benzene.

Lifetime Results

The observation of nonexponential decays in all the benzene complex systems studied is not surprising in view of the presence of more than one emitting species. Indeed, what is surprising is the observation by Simons and coworkers of an exponential decay in his benzene-chloroform system.[55] They attribute this to the difference in intermolecular vibronic coupling and complex pair orientation and fluctuation in the solvent cage.[53] Although Simons has identified two emitting species from his absorption and phosphorescence spectra, he curiously ignores these as possible causes of the nonexponentiality.

It appears possible that Simons and coworkers did not observe any nonexponentiality in the benzene-chloroform-d complex because of experimental conditions. Although chloroform and chloroform-d show the same complexing strength toward benzene,[50] the emission intensity from the chloroform-

Figure 14. Plot of relative intensity versus wavelength for the 0,0 band of C_6H_6-$CDCl_3$

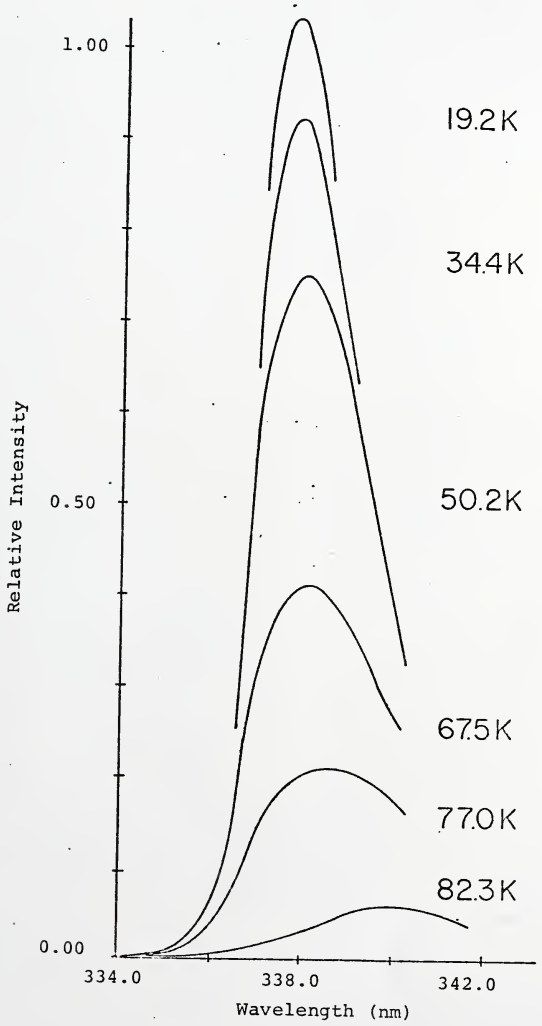
1.00
0.50
0.00
Relative Intensity
19.2K
34.4K
50.2K
67.5K
77.0K
82.3K
334.0
338.0
342.0
Wavelength (nm)

d-benzene system is two to three times that of the chloroform-benzene system.[53] If the nonexponentiality were due to the overlapping decays of the 2:1 and 1:1 chloroform-benzene complexes and the enhanced intensity of the chlororform-d complex versus the chloroform complex were predominantly due to the 1:1 complex, one might expect to observe a nonexponential decay in the chloroform system and an exponential one in the chloroform-d system. The fact that our cooling procedure produces both complexes about equally whereas Simons' technique favors the 1:1 chloroform-benzene complex is consistent with the above assumptions and conclusions.

The identification of the origin of the different components of our nonexponential decays to specific complexes is not easy, although Simons' previous work is again helpful. He has measured a phosphorescence lifetime of 1.7 seconds for the benzene-chloroform-d system in 3MP at 77K.[53] This is in reasonably good agreement with our long-lived component for the same system (2.2 seconds). The difference is most probably due to a small temperature difference in the two experiments. Figures 11 and 13 show that at ~77K both components of our phosphorescence decay are very sensitive to temperature. Because Simons was observing the decay of the 1:1 complex, it is reasonable to conclude that our long-lived component originates from the 1:1 chloroform complex and the short-lived component from the 2:1 chloroform complex.

From a comparison of the average lifetime and phosphor-

escence efficiency of the chloroform-benzene complex with that of the chloroform-d complex, Simons has concluded that the difference in lifetimes at 77K is due to a difference in the nonradiative decay rates for the two complexes. This was interpreted as evidence for an intermolecular vibronic coupling between the C-H(D) motion in chloroform(-d) and the benzene ring.[53]

From our results in Tables 2 and 3, it is possible to explore further the reasons for the difference in the nonradiative decay rates. The low temperature decay rate, k_{10}, is seen to be the same, within experimental error, for both the chloroform and chloroform-d complexes. Thus the combined radiative and nonradiative decay rate from the lowest triplet to the ground state is unaffected by the complexing partner, chloroform or chloroform-d. The large differences observed for ΔE_{21} and k_{20} for the two complexes show, however, that it is some level above T_1 (here labeled T_2) in equilibrium with T_1, to which or through which radiationless processes may occur at higher temperatures ($T \geq 77K$). We propose that the T_2 level is simply the potential barrier over which the complexed benzene must pass to form a substituted hexatriene. The hexatriene formation step is envisaged as occurring via a concerted mechanism involving the chloroform and/or solvent and the triplet benzene and it is this hexatriene precursor that is deuterium sensitive.

There are a number of observations which support this model as the major pathway of radiationless decay in benzene.

1) Simons and coworkers have observed that upon irradiation of benzene in 3MP at 77K, solvent-substituted hexatriene is formed. Similar experiments with chloroform-complexed benzene yielded chloroform-substituted hexatriene while with chloroform-d complexed benzene, solvent-substituted hexatriene was formed, although at a slower rate than for uncomplexed benzene in 3MP.[50,55] As Simons points out in justifying his intermolecular vibronic coupling model, the Franck-Condon overlap factor for the chloroform-d-benzene complex is expected to be smaller than that for the chloroform complex.[53] Thus, the probability of energy exchange necessary for chloroform-substituted hexatriene formation is decreased or prohibited in the chloroform-d-benzene complex. 2) The increase observed in ΔE_{21} for either lifetime component upon substitution of chloroform-d (see Table 2 or 3) is consistent with the contention that the CH(D) fragment is the important energy acceptor since upon deuteration the zero point energy of the complex is expected to decrease. Simons and coworkers have also noted that the phosphorescence intensity of the chloroform-d-benzene system is two to three times more intense[53] than the chloroform one. This again is just a consequence of the larger activation energy (ΔE_{21} of the 1:1 complex) needed in the chloroform complex. 3) Substituted hexatrienes are apparently formed in the triplet manifold[53] and are known to be formed via a one photon process.[45] They also show an external deuterium isotope effect in their formation.[50,53,55] 4) The large values of

k_{20} found previously for benzene phosphorescence decays in many different solvents cannot be explained by current theories (e.g., Lin's)[9] of intramolecular radiationless processes. 5) No other one-photon processes (including isomerization)[31] are known to occur in glasses containing benzene.

It has been implied in the above discussion that there exists only one potential barrier, T_2, to substituted hexatriene formation. There are several pieces of data which indicate, however, that several such barriers (i.e., processes) are possible. First is the previously discussed observation of Simon's on the chloroform-substituted and solvent-substituted hexatriene formation from irradiation of chloroform and chloroform-d complex systems, respectively. That two different types of photoproducts can be formed from the 1:1 complex implies that the complex is more properly viewed as a 1:1:1 chloroform-benzene-solvent complex. Thermal activation of chloroform-benzene-solvent exciplex would preferentially result in the chloroform-substituted hexatriene because of a larger Franck-Condon overlap between benzene and the C-H molecular fragment of the chloroform versus the solvent as evidenced by the larger 0,0 transition in complexed versus "uncomplexed" benzene. Deuterating the chloroform causes the process leading to chloroform-substituted hexatriene to be more difficult because of the smaller Franck-Condon factor in C-D versus C-H and actually results in the reaction with the C-H molecular fragment of the solvent becoming more efficient than reaction with the C-D molecular fragment of the chloroform-d. Each exciplex

should then possess at least two barriers corresponding to benzene reaction with either of its partners. The higher energy associated with T_2 in chloroform-d versus chloroform (see Tables 2 and 3) may then reflect not just a lowering of the zero point energy of the exciplex due to deuteration, but also the larger barrier to solvent versus chloroform-substituted hexatrienes. We will return to the question of whether or not benzene can form an exciplex with the solvent later.

The second piece of evidence for additional processes is more direct and comes from the temperature dependence of the phosphorescence lifetimes of the "benzene-chloroform" complex. The experimental lifetimes as shown in Figures 10 and 12 are substantially shorter than those predicted on the basis of the fit to the data and indicate the need for a second Arrhenius type term (i.e., $k_{31}e^{-\Delta E_{31}/kT}$) to describe the data. Unfortunately, the lifetimes may not be followed to sufficiently high temperatures to allow the calculation of the parameters k_{31} and ΔE_{31} but the need for this second term is evident. It is significant that this T_3 shows up in the 1:1 "chloroform-benzene" complex as it is precisely in this case that we would predict that it should be possible to transfer energy to the C-H fragment of either the solvent or the chloroform.

The proposal that benzene can form a triplet exciplex with the solvent requires some justification. Not only does such a proposal appear reasonable from the present results,

but it is consistent with other previous studies of "uncomplexed" benzene and its methyl derivatives in hydrocarbon solvents. Simons[55] has shown that benzene in ethanol (and its various deuterated forms) exhibits an intermolecular coupling which is specific to the methyl hydrogens rather than the hydroxyl hydrogen. Nieman and coworkers have done a great deal of research on temperature dependence of the phosphorescence lifetimes of benzene and its methyl derivatives in many different solvents. They have observed that the k_{10} values vary appreciably for different solvents, even for the so-called inert alkane solvents (see Table 5).[31,56] They have further noted that 1) methyl substitution in deuterated benzene causes an essentially linear increase in k_{10}, 2) the relative decay rates (k_{10}[solute:solvent]/k_{10}[C_6D_6:same solvent]) are solvent independent, and 3) the relative decay rates (k_{10}[solute:solvent]/k_{10}[same solute:C_7F_{14}]) are constant for any solute despite the fact that the magnitude of the solvent effects is a function of methyl substitution. These data which are solely concerned with the decay rate from the lowest emissive triplet are all consistent with the idea of a benzene-solvent exciplex from which emission occurs.

Theoretical Calculations on the Exciplex Model

Results of Open and Closed Shell INDO Calculations

The computer program used for the INDO calculations was supplied by the Quantum Chemistry Exchange Program

Table 5
Reported Parameters Determined from Benzene Decay Rates in Different Solvents (Form I)

Solute	Solvent[a]	$\Delta E_{21}(cm^{-1})$	k_{20}	k_{10}
C_6H_6	C_6H_{12} (M)	450	$7.5x10^{+2}$	.096
C_6D_6	C_6H_{12} (M)	580	$2.7x10^{+3}$	.061
C_6H_6	C_6H_{12} (S)	570	$4.6x10^{+3}$	.091
C_6D_6	C_6H_{12} (S)	800	$1.0x10^{+4}$	.071
C_6H_6	3MP[b]	960	$1.1x10^{+7}$	.113
C_6H_6	Ethanol	1540	$7.4x10^{+9}$	.115
C_6H_6	C_7H_{14} (unannealed)	1160	$2.8x10^{+8}$	.100
C_6H_6	C_7H_{14} (crystal)	720	$6.2x10^{+3}$	.070
Toluene	C_7H_{14} (crystal)	480	$3.2x10^{+2}$	.094
Toluene-d_8	C_7H_{14} (crystal)	670	$3.1x10^{+2}$	.072
C_6H_6	C_7F_{14} (unannealed)	520	$2.5x10^{+3}$	.073
C_6D_6	C_7F_{14} (unannealed)	890	$1.4x10^{+5}$	.044
Toluene	C_7F_{14} (unannealed)	820	$4.8x10^{+4}$	.079
Toluene-d_8	C_7F_{14} (unannealed)	1060	$7.5x10^{+4}$	.060
Mesitylene	C_7F_{14} (unannealed)	730	$3.5x10^{+3}$	.078

[a] see reference 31

[b] see reference 59

(QCPE #141) and originally written by P. Dobosh.[60] It will do open or closed shell INDO calculations for atoms H through F and is a modified version of a program described by Pople and Beveridge.[61]

We have investigated theoretically the potential of triplet benzene to complex with an alkane solvent by doing open shell, semi-empirical INDO calculations on this system. As a model we chose to study the interaction of triplet benzene with a hydrogen molecule. The bonding in a hydrogen molecule can be likened to that of a C-H bond of an alkane without the computational problems introduced by steric factors caused by "inert" parts of the solvent molecule. We have also carried out closed shell INDO calculations on the interaction of ground state benzene with H_2 in order to compare the tendency of the S_0 and T_1 states of benzene to interact with the solvent. Further, we have done open shell INDO calculations on the triplet benzene-hydrogen fluoride system (fluorine approaching the aromatic ring) to see if the apparent inertness of the fluorocarbons toward triplet benzene is predicted by the computations. In this way we could check the applicability of INDO calculations to this system, as well as defend our choice of model system.

In considering the interaction of the hydrogen molecule with benzene triplet, H_2 was allowed to approach from above the plane of the benzene ring as this would optimize the H_2 interaction with the pi electron cloud and is also

consistent with the probable geometry of the benzene-chloroform complex as determined by Simons.[52,53] The line joining the H-H bond was kept perpendicular to the plane of the benzene ring since steric considerations in alkanes would prohibit any other type of approach. There are then three different ways in which H_2 may approach: (Figure 15) from above a particular carbon atom (approach A), from above the center of a carbon-carbon bond (approach B), or from above the middle of the ring along the C_6 axis (approach C).

Table 6 is a compilation of the results of the INDO calculation for these different lines of approach. r is the distance of the first H atom above the ring (the second H atom is kept at the equilibrium bond distance .74611 Å from the first). E is the total energy of the molecule in Hartrees. The remaining three columns are the valence electron densities of the primary interacting atoms (i.e., the two H atoms and the nearest interactive carbon atom) and are given in order to illustrate how the electron density of the complex changes as a function of distance. Figure 16 is a plot of r versus E for each of the different lines of approach and graphically illustrates the interaction of H_2 and benzene triplet.

Table 7 is a compilation of the results for the interaction of ground state benzene with H_2 for the approaches that lead to the strongest and weakest interactions in the triplet state. Figure 17 is a plot of r versus E for these lines of approach. Similarily Table 8 is a compilation of

Figure 15. Approach of hydrogen molecule to triplet benzen

Approach

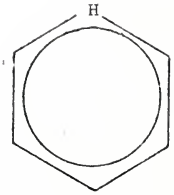

A

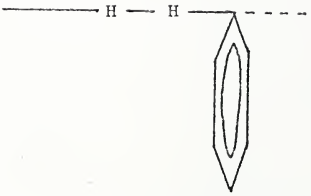

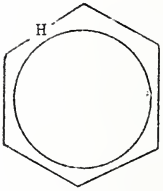

B

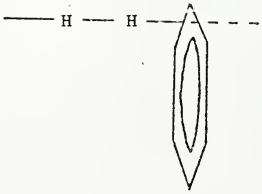

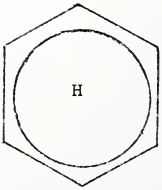

C

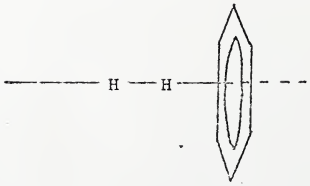

Table 6
Results of INDO Calculations on H_2-C_6H_6 Exciplex

Approach*	r (Å)	Total Energy (Hartrees)	Valence Electron Denisty		
			H^1	H^2	C (nearest)
A	.75	-46.474	0.88	1.14	3.91
	1.00	-46.821	0.94	1.13	3.87
	1.25	-46.869	1.03	1.11	3.84
	1.50	-46.827	1.14	1.08	3.84
	1.75	-46.780	1.13	1.06	3.90
	2.00	-46.745	1.08	1.03	3.96
B	.75	-46.668	0.84	1.13	3.84
	1.00	-46.821	0.96	1.11	3.83
	1.25	-46.844	1.15	1.09	3.84
	1.50	-46.817	1.17	1.07	3.88
	2.00	-46.745	1.09	1.03	3.94
C	.75	-46.790	1.12	1.07	3.94
	1.00	-46.802	1.12	1.05	3.94
	1.25	-46.791	1.11	1.04	3.95
	1.50	-46.768	1.08	1.03	3.96
	2.00	-46.726	1.03	1.01	3.97

Energy C_6H_6 (triplet) =-45.290

Energy H_2 = -1.475

Total Energy System =-46.765

*see Figure 15

Figure 16. Plot of H_2-C_6H_6(triplet) exciplex energy versus intermolecular distance for different complex geometries

O = Approach A

Δ = Approach B

□ = Approach C

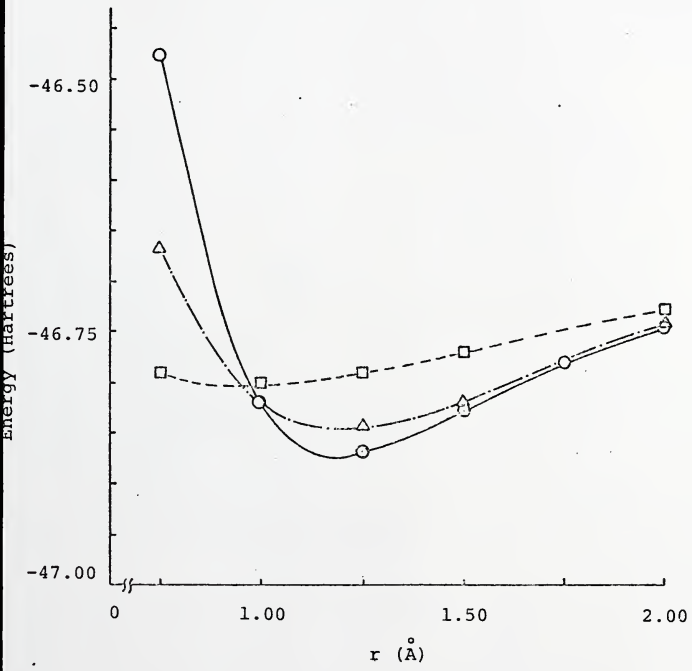
-46.50
-46.75
-47.00
Energy (Hartrees)
0
1.00
1.50
2.00
r (Å)

Table 7
Results of INDO Calculations on H_2-C_6H_6 Ground State Complex

Approach*	r (Å)	Total Energy (Hartrees)	Valence Electron Density		
			H^1	H^2	C (nearest)
A	.75	-46.448	0.63	1.34	3.91
	1.00	-46.868	0.73	1.31	3.90
	1.25	-47.010	0.83	1.23	3.92
	1.50	-47.051	0.90	1.14	3.94
	2.00	-47.057	0.97	1.04	3.97
C	.50	-46.804	0.66	1.39	3.98
	.75	-46.908	0.73	1.32	3.98
	1.00	-46.982	0.81	1.24	3.98
	1.50	-47.045	0.93	1.10	3.97
	2.00	-47.053	0.98	1.03	3.97

*see Figure 15

Energy C_6H_6 (ground state)	= -45.576
Energy H_2 (ground state)	= -1.475
Total Energy	= -47.051

Figure 17. Plot of H_2-C_6H_6 (ground state) complex energy versus intermolecular distance for different complex geometries

O = Approach A

□ = Approach C

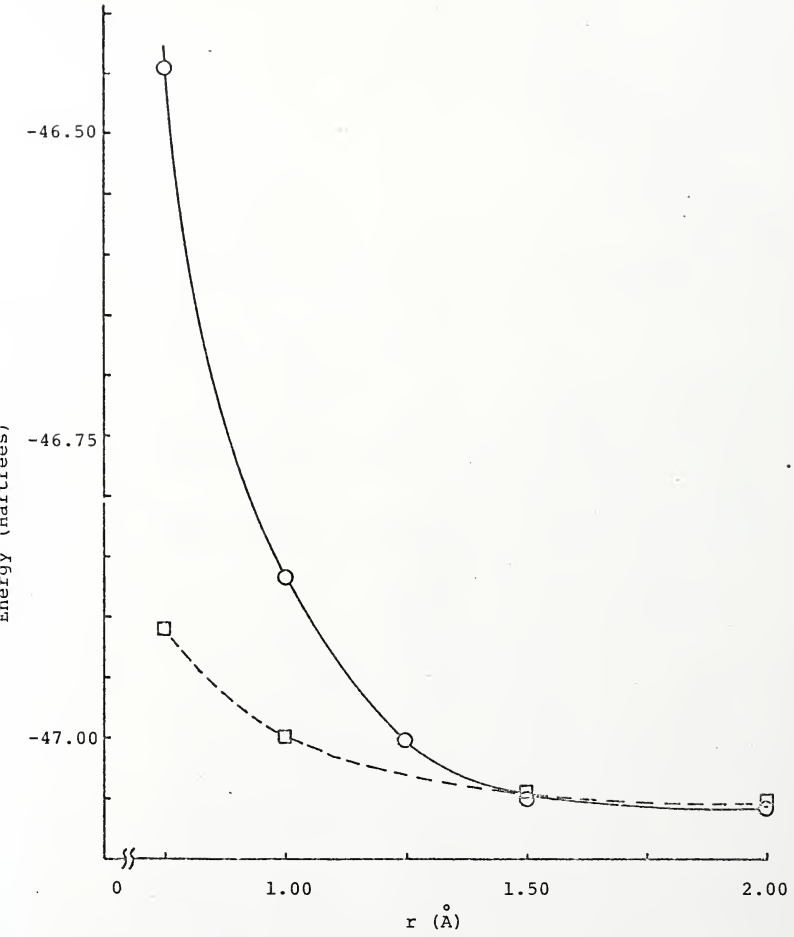
-46.50
-46.75
-47.00
Energy (hartrees)
0
1.00
1.50
2.00
r (Å)

the results for the interaction of triplet benzene with HF (F approaching first) for the approach from above a carbon atom. Figure 18 is a plot of r versus E for these different interactions.

One last set of calculations was performed in which the most stable H_2-benzene configuration was chosen; the second H atom was moved such that the hydrogen molecule was parallel to the aromatic ring. The second H atom was then rotated about the first in order to see if there might be - steric considerations aside - a more stable configuration than the one chosen which could act as a driving force to bring the H_2 (or C-H for an alkane) into a position from which concerted solvent-substituted hexatriene formation might occur. The results are tabulated in Table 9; Figure 19 is a plot of E versus rotation angle for the various configurations tested.

Discussion

The results for the interaction of triplet benzene and H_2 clearly indicate that these species will complex with each other (see Figure 6). The energy of interaction is approximately 0.1 Hartree and is much larger than we would qualitatively expect even for a model that essentially ignores steric factors. It is significant that benzene in its ground state shows no analogeous interaction (see Figure 17) indicating the true exciplex character of the complex. That the strongest exciplex is formed with H_2 over a particular carbon atom rather than along the C_6 axis

Table 8
Results of INDO Calculations on HF-C_6H_6 Exciplex

Approach*	r (Å)	Energy Total (Hartrees)	Valence Electron Density		
			H	F	C (nearest)
A	.75	-69.059	1.20	6.80	3.42
	1.00	-71.642	1.19	6.96	3.62
	1.25	-72.378	1.16	7.08	3.73
	1.50	-72.469	0.99	7.11	3.86
	1.75	-72.441	0.76	7.19	3.96
	2.00	-72.414	0.73	7.24	3.97

*see Figure 15

Energy C_6H_6(triplet) = -45.290
Energy H-F(g.s.) = -27.108

Total Energy = -72.398

For H-F:
Valence Electron Density H = 0.72
Valence Electron Denisty F = 7.28

Figure 18. Plot of HF-C_6H_6(triplet) exciplex energy versus intermolecular distance for different complex geometries

O = Approach A

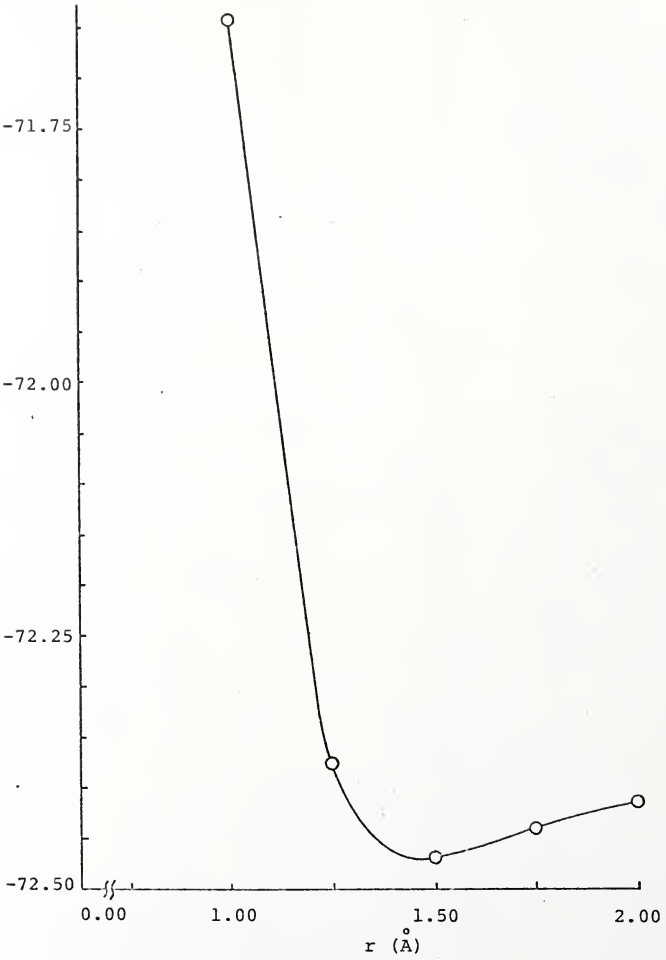
-71.75
-72.00
-72.25
-72.50
0.00
1.00
1.50
2.00
r (Å)

Table 9
Results of INDO Calculations on Stablest H_2-C_6H_6 Exciplex as a Function of Angle

Angle (°)	Total Energy (Hartrees)	Valence Electron Density		
		H^1	H^2	C (nearest)
0	-46.888	1.04	1.16	3.78
60	-46.893	1.04	1.16	3.79
90	-46.897	1.05	1.16	3.78
120	-46.894	1.07	1.15	3.78
180	-46.885	1.09	1.15	3.78

Figure 19. Plot of H_2-C_6H_6(triplet) exciplex energy versus relative intermolecular orientation

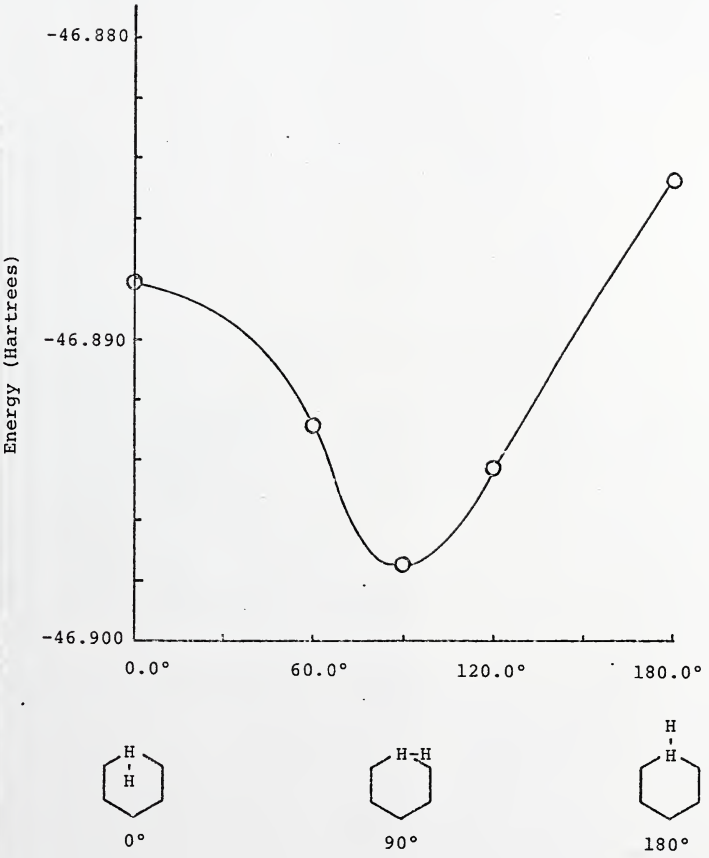
-46.880
-46.890
-46.900
Energy (Hartrees)
0.0°
60.0°
120.0°
180.0°
H
H
H-H
H
H
0°
90°
180°
Angle (°)

of the molecule may be surprising at first sight but an inspection of the molecular orbitals[62] of benzene (see Figure 20) provides a ready rationalization. For triplet benzene there are two electrons in the a_{1u} molecular orbital (m.o.), three in the two e_{1g} m.o.'s and one in the two e_{2u} m.o.'s. As Figure 20 clearly indicates, there is a node along the axis of benzene for both the e_{1g} and e_{2u} m.o.'s and hence there can be no positive overlap of these orbitals with any molecule approaching along this line. Approach from above, say, carbon two, offers the potential for a strong interaction with these orbitals, as does approach from above a carbon-carbon bond. Only the a_{1u} m.o. offers the possibility for positive overlap with the H_2 molecule and apparently this overlap, while sufficient to maintain a relatively weak interaction (0.04 Hartrees) in the triplet state, is not capable of maintaining a bond in the ground state.

Interestingly, the HF molecule showed about the same tendency to complex with triplet benzene as did H_2. The HF complex is apparently weaker than the H_2 complex as its interaction energy is only about 0.07 Hartree for the stablest configuration; however, the most significant result of this calculation can be seen by studying the valence electron densities. These two complexes are very different in character. An examination of Table 8 reveals that the fluorine atom in the complex is positive relative to what it is in HF. While it is unclear whether F is actually

Figure 20. Molecular orbitals of benzene (the wave-functions in the cross-hatched regions are out of phase with those in the plain regions)

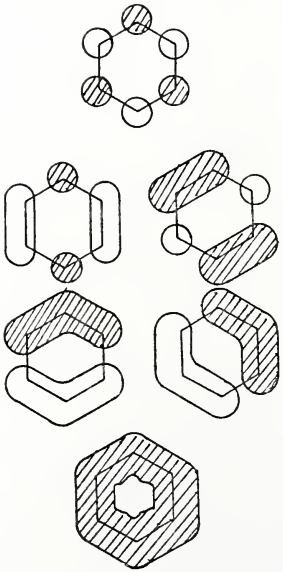

adapted from reference 62.

donating electron density to the benzene ring (F is slightly negative at 1.25 Å) this situation is in contrast with H_2 (see Table 6) in which it is the ring that clearly donates electron density to the H_2. This means that H_2 must accept electron density into an antibonding orbital of the molecule and thus complexing weakens the H-H bond. This is an important result in explaining the photochemical activity of the benzene triplet manifold in alkane solvents as it is the C-H bond of the solvent that must be broken in order to form the solvent-substituted hexatriene. (It is this same C-H bond that is broken in the two photon process that gives the solvent radical in glasses containing benzene.) Further, benzene in fluorocarbons should show either less photochemical activity as there is less tendency to populate an antibonding orbital of HF, or a very different photochemical activity if F donates electron density to the aromatic ring. This latter alternative would entail the use of a filled p or sp hybrid orbital that should have little effect on the HF bond strength. While little is known of the photochemistry of benzene in fluorocarbons, these conclusions appear to be consistent with current experimental results.[31] Thus, while our theoretical study of HF and benzene triplet shows that complex formation is likely, this complex is expected to behave very differently from the one involving H_2 and is, therefore, not inconsistent with experimental observations. The idea of a benzene-fluorocarbon complex is an intriguing one since the k_{10} values for benzene do vary from one

fluorocarbon solvent to another,[51] although they are about the same value as those found in rare gas matrices.[56] Benzene still shows a strong temperature dependence in fluorocarbons[31] and Nieman has observed that on going from benzene to toluene the parameters describing T_2 increased in the case of methylcyclohexane (crystalline phase) while they decreased in the case of perfluoromethylcyclohexane (unannealed glass form).[31] This opposite trend for hydrocarbon versus fluorocarbon solvents when substituting into the benzene ring would be expected on the grounds that benzene is an electron donor in one case and an electron acceptor in the other. There is, however, too few data on fluorocarbons to say whether this is a general trend or not.

The last set of calculations involving H_2 above and parallel to the benzene ring, shows the most stable complex configuration to be one in which the hydrogen molecule lies above and at a slight angle to a C-C bond (see Figure 19). This is significant as it shows the relative stability of a configuration that is a reasonable transition state for the concerted process leading to substituted hexatriene. Since this transition state in an alkane should be destabilized by steric factors, it is a likely candidate for T_2. Moreover, the difference in energy between the most and the least stable configuration is only about 0.01 Hartree (about 2000 cm^{-1}). Thus, it is apparent that this type of rotation involves energies of the same order of magnitude as the energy

difference between T_1 and T_2. Such a configuration for T_2 would naturally be sensitive to environment, again as observed.

Comments on Possible Exciplex Formation in Other Phases

Reactions similar to those that occur at low temperatures apparently persist even in the gas phase. Semeluk and Unger[63-65] have shown that benzene in the triplet state[63] is responsible for the photochemical rupture of the C-H bond in chloroform in the gas phase.[63,64] The rupture of the energetically stronger C-H bond versus the weaker and more numerous C-Cl bonds, is consistent with the involvement of an intermediate complex whose nature can easily be envisioned as similar to the low temperature benzene chloroform complex.

For liquids, benzene is known as a radiation shielder for a number of materials. The introduction of benzene into liquid hydrocarbons[66,67] and alcohols[68] prevents or shields the C-H bonds of the solvents from rupturing upon exposure to gamma irradiation while there is no effect on the benzene. The protection mechanism probably involves energy transfer to the benzene, followed by radiationless deactivation via collisions in the solution. This transfer occurs in glasses at low temperatures and results in solvent radical formation. The benzene will not be affected by this energy in liquids because it has many new radiationless channels

open to it - such as dimer formation - through which it can lose this energy.

While benzene is not known to phosphoresce in liquid solutions, other materials that can accept benzene triplet energy can be used to monitor the amount of triplet benzene present. Thus, the isomerization of cis-butene-2 has been used[69] to show that the yield of triplet benzene in a cyclohexane solution depends on a process with an activation energy of 785 cm^{-1} and a preexponential factor of $3.4 \times 10^{+8}$ s^{-1}. Both these values are similar[70] to those determined from the lifetime results for benzene in various alkane solvents at low temperatures.[21-24,31] While the experimental results have been interpreted in terms of an activation energy for intersystem crossing, the data are also consistent with the idea that the butene isomerization process may monitor the T_2 level of triplet benzene or may itself accept the triplet energy through a T_2-type state of its complex with triplet benzene. This question will be difficult to resolve.

Some work in the liquid and gas phases on benzene pose problems to our interpretation of the solid phase data. Wilzbach, Harkness and Kaplan[35] showed that benzene-1,3,5-d_3 in the vapor phase or in liquid solutions, will, when subjected to 254 nm light, isomerize to give various trideuteriobenzenes. This was taken as conclusive proof for the presence of an intermediate excited state isomer of benzene that can decay to benzene in the ground state. Such an isomerization pathway cannot be used to explain much of the

data on the T_2 state at low temperatures since this isomerization reaction (1) has not been found in solid solutions,[31] (2) apparently occurs in the singlet manifold of benzene,[34,35] and (3) is probably not meaningful in view of the k_{10} results of Nieman, we have discarded it as an alternative to our proposal.

It should be pointed out that the apparent correlation of the reactions of benzene in the different phases indicates that the complexing tendency is fairly large and very fast. The gas phase results show that the complex can be collisional in nature and this may well be the most accurate way of viewing the complex in the solid phase as well. Thus, with the benzene locked into a solvent cage with some other molecule, it may undergo multiple collisions which will effectively appear as one long complex. These two alternatives will be difficult to distinguish from one another and may simply represent opposite sides of the same coin.

In conclusion, it is hoped this work will not only introduce new avenues of approach to the many-sided benzene problem, but may also change our thinking as to what constitutes a truly inert solvent.

CHAPTER III
DURALDEHYDE IN DURENE

Introduction

Duraldehyde Phosphorescence

Reagent grade durene (1,2,4,5-tetramethylbenzene) exhibits a blue emission whose spectral characteristics indicate that it originates from an aldehydic impurity.[71,72] In 1970, Fischer confirmed this hypothesis by synthesizing duraldehyde (2,4,5-trimethylbenzaldehyde), doping it into a durene lattice, and showing its phosphorescence equivalent to that of the impurity.[73] Fischer also analyzed the 4K duraldehyde phosphorescence and concluded that it originated from a $^3n\pi^*$ state, although it did contain many characteristics of a $^3\pi\pi^*$ state. Indeed, the literature on this subject contains a number of conflicting assignments for the lowest triplet of duraldehyde. Sharnoff[74] determined the zero-field splitting parameters for triplet duraldehyde in durene and from their magnitude decided that the lowest state was $^3n\pi^*$. He also determined the lifetime as 33±5ms, a value consistent with this assignment. Recently, Hanson and Sheng[75] observed the Stark splitting for the lowest triplet state and concluded that it was supportive of a lowest $^3\pi\pi^*$ state assignment. Hirota and coworkers have observed the ESR,[76,77] PMDR,[77-79] and temperature dependence of the duraldehyde

phosphorescence[80] from which they concluded[81] that triplet duraldehyde can be best represented as a mixture of $^3\pi\pi^*$ and $^3n\pi^*$ states (i.e., $0.99|^3\pi\pi^*>+0.14|^3n\pi^*>$).

In a temperature-dependence study of duraldehyde phosphorescence Migirdicyan[82] has recently observed the increase in intensity with temperature of several bands to the blue of the low temperature origin. Vibrational bands of $1684cm^{-1}$ were also observed to grow in intensity with temperature. This temperature dependent emission was ascribed to a thermally populated $^3n\pi^*$ state lying above the lowest $^3\pi\pi^*$ state. Dual phosphorescence from both $^3n\pi^*$ and $^3\pi\pi^*$ states in the same molecule was claimed to be possible at high enough temperatures.

Duraldehyde Photochemistry

Two primary photoproducts have been identified after the irradiaiton of duraldehyde in a durene host. Migirdicyan[83] was the first to observe that duryl radical, occurring via a one photon process, formed upon photolysis. The triplet state origin of this process was implied in this work.[83] It was found that duryl radical formation required an induction period for temperatures below 300K. Between 120K, the lowest temperature where radicals were observed, and 160K, the temperature where duraldehyde ceases to emit, the results were sample dependent showing that the thermal history and treatment of the sample had a strong influence on radical formation.[83] From a plot of rate of radical

formation versus inverse temperature, it was found[83] that this process required an activation energy of 600±80 cm^{-1}.

In a separate study,[84] Migirdicyan showed that a photoenol was produced upon irradiation of duraldehyde in durene. The photoenol formed was shown to absorb exclusively parallel to the C' durene crystal axis. From a plot of initial rate of enol formation versus inverse temperature, it was found that this photoproduct was formed by two processes. The first, which dominated in the 160 to 215K range, required an activation energy of 4.0 kcal/mole (1400 cm^{-1}) while the second, higher temperature (215 to 300K) process required an activation energy of only 1.6 kcal/mole (560 cm^{-1}).[84]

Durene Crystal Structure

The durene lattice contains two crystallographically inequivalent molecules per unit cell.[85] A detailed analysis of the durene crystal structure by Stam[86] showed two unusual features. First, the hydrogens on adjacent methyl groups have an eclipsed conformation with two hydrogens on each methyl pointing toward each other and with the two farthest distant from each other lying in the molecular plane (see Figure 21). The eclipsed hydrogens (numbers 2 and 5, numbers 3 and 6) are only 2.4 and 2.5 Å from each other. This structure, which is probably not the most stable isolated molecule conformation, is the result of strong intermolecular forces. Second, the environment about each of these methyls is different: in one, each of the three hydrogens is 2.6 or

Figure 21. Conformation of durene in its lattice

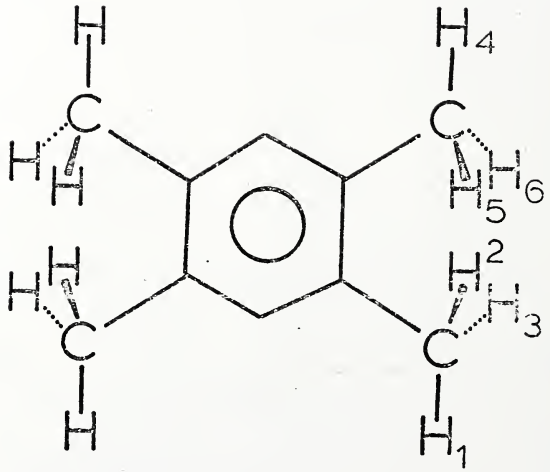
H
C
H
H
H
C
H
H
H
H4
C
H5
H6
H2
H3
C
H1

2.7 Å from a hydrogen of an adjacent durene molecule, whereas in the other, only two of the hydrogens (the two non-planar ones) are within 2.7 Å of a hydrogen on a neighboring durene. The two remaining methyls in durene are related to the above two via a symmetry operation. These unusual features may be decisive for the determination of the most probable substitution site and conformation of the duraldehyde molecule in the durene host lattice. That the duraldehyde does substitutionally replace a durene molecule in the lattice has been shown by both Sharnoff[74] and Fischer.[73] In his triplet state ESR measurements,[74] Sharnoff found two signals which he attributed to triplet duraldehyde in two magnetically inequivalent sites. In his 4K phosphorescence study, Fischer[73] saw a doubling of most bands with the weaker lower energy peak of the doublet 23 cm^{-1} from the upper one. He surmised that this doubling arose because of a crystalline site effect.

Dissertation Work

Although a large amount of work has been reported on the duraldehyde in durene system, no comprehensive, coherent picture of the photophysical and photochemical processes has emerged. Neither has any consensus on the assignment of the lowest triplet of duraldehyde been reached. To gain additional knowledge on these important topics, we have studied in detail the temperature dependence of both the phosphorescence lifetime and intensity of duraldehyde in durene in

this dissertation. We have further observed the temperature dependence of the infrared spectrum in the critical carbonyl stretching region and have observed the effects of ultraviolet photolysis on the intensity of these bands. From these data we have formulated a coherent kinetic model for the dissipation of duraldehyde triplet energy which is consistent with previous existing results. Finally, we have proposed a comprehensive model which describes all known photophysical and photochemical processes occurring via the duraldehyde triplet manifold.

Experimental Procedure

Crystals of durene (Eastman Organic Chemicals, practical grade) containing duraldehyde as a natural impurity (10^{-3} g/g) were grown by two different procedures. In the first, durene was slowly recrystallized from benzene while in the second a durene melt was slowly allowed to recrystallize in a Bridgman furnace. Except for a somewhat larger overall phosphorescence intensity for crystals taken from the top of the melt where duraldehyde was apparently concentrated, there was no apparent effect of crystal source on the results. Only the second technique produced crystals large enough to be used in the infrared work.

The major experimental problem in handling the duraldehyde in durene system is caused by the strong tendency of durene to sublime even at low temperatures. Thus, for both

the temperature-dependent phosphorescence intensity and infrared work it was necessary to isolate the durene crystal from the vacuum inside the closed cycle helium dewar. For the phosphorescence intensity and lifetime work we used essentially the same sample cell used in the benzene work (see Figure 4). The durene crystal was first mounted on a copper plug which was then inserted into the cavity of the sample holder. Modelling clay was used to hold the crystal in place and a curved suprasil cover was then inserted into the clay to produce a vacuum-tight seal that prevented the durene from subliming. Emission was viewed at right angles to the excitation beam. For the infrared work a hole 1/8" by 3/8" was cut in the copper plug to allow the IR beam to pass through. The cell holder in this instance was further modified to have front and rear windows to allow the IR to pass. The window material was changed from quartz to KBr.

For the phosphorescence work, crystals were irradiated with 313 nm light by passing the output of the 1000 watt xenon arc lamp through filter solutions (5 cm .178 M $NiSO_4$, 5 cm 4.0×10^{-4} M K_2CrO_4, 1 cm .0245 M potassium biphthalate 3 mm Corning glass filter 7-54). Slits for the phosphorescence intensity work were typically 20 to 30 microns (bandpass 0.02 to 0.03 nm) at low temperatures and, at most, 200 microns (bandpass 0.4 nm) at the highest temperatures. For lifetime work slits varied from 100 microns (bandpass 0.2 nm) at low temperatures to around 1000 microns (bandpass 2.0 nm)

at the highest temperatures.

For the infrared work a grating infrared spectrometer (Perkin-Elmer 621, resolution: $\pm$ 1 cm^{-1}) was used. A closed cycle helium dewar (Air Products Displex) was again used to cool the sample, but temperatures were monitored with a digital temperature readout (Cryogenics Technology, Inc., reading $\pm$ 0.1K). The temperature could not be controlled. Infrared runs, with or without irradiation, were thus made as the sample warmed up. The temperature changed less than 2K during an IR run and typically varied by 20-40K for one hour of irradiation. Samples were irradiated using either a 1000 watt xenon arc lamp or a 1000 watt high pressure mercury vapor lamp whose output was passed through a filter (Corning glass filter 7-54) which passes light in the 250 to 390 nm spectral range. The irradiation produced no visual change in the KBr discs, but the crystals were unable to withstand more than 3 to 5 hours of irradiation without fracturing. Crystals were of sufficient dimension to entirely cover the aperture in the copper plug and were normally about 1 mm thick.

Experimental Results

Phosphorescence Spectra

The phosphorescence spectrum of duraldehyde in single crystal durene at 11K is shown in Figure 22. This result agrees with the 4K spectrum of Fischer[73] except that our

Figure 22. Phosphorescence spectrum of single crystal duraldehyde in durene at 11K

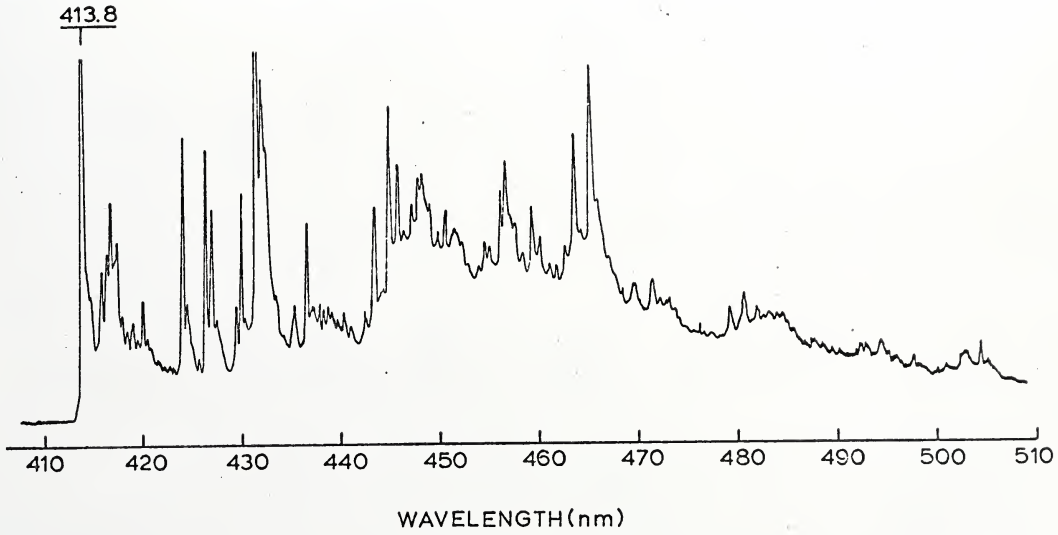
413.8
410
420
430
440
450
460
470
480
490
500
510
WAVELENGTH(nm)

spectrum shows the doubling of more bands. Most of our low energy components of the doublets are substantially broadened compared with Fischer's work. Figure 23 shows the temperature dependence of the high energy bands of the phosphorescence spectrum and clearly illustrates that two new bands, one at 411.2 nm and the second at 408.0 nm, increase with temperature. The site splitting is no longer resolvable by 50K. Figure 24 is a plot of the natural logarithm of intensity of the peak height of the 431.6 nm band and the 411.2 nm band (most prominent of the two bands that grow in at higher energies) versus inverse temperature. Figure 25 is a similar plot of the natural logarithm of intensity versus temperature. These figures illustrate the manner in which the overall intensity decreases as a function of temperature (indicated by the 431.6 nm band) as well as the behavior of the 411.2 nm band which first increases and then decreases in absolute intensity. The 408.0 nm band behaves similarly to the 411.2 nm band but it first appears at a higher temperature than the 411.2 nm band (65K versus 40K) and never achieves a very large absolute intensity, although it is nearly as intense as the 411.2 nm band by 146K.

Phosphorescence Lifetimes

Phosphorescence lifetimes at different temperatures were recorded for the 413.8 nm and 431.6 nm bands as well as the 408.0 and 411.2 nm bands of the higher energy emission. At a given temperature all bands gave the same lifetime

Figure 23. Temperature dependence of the duraldehyde in durene phosphorescence spectrum

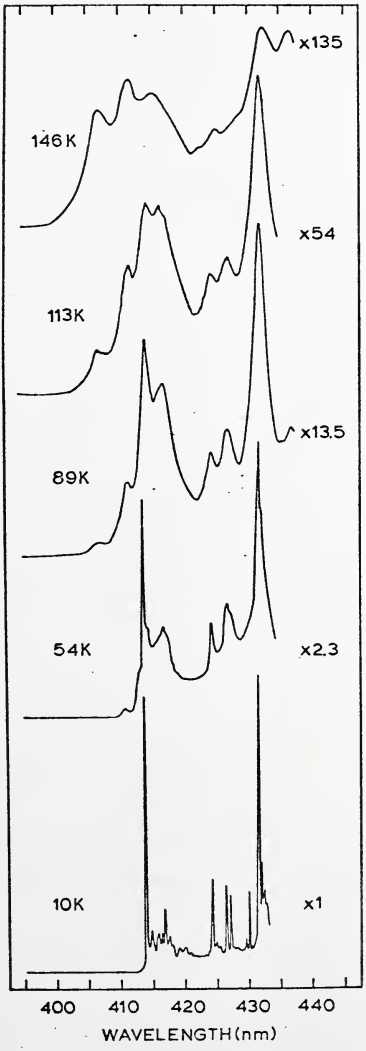
x135
146K
x54
113K
x13.5
89K
54K
x2.3
10K
x1
400
410
420
430
440
WAVELENGTH(nm)

Figure 24. Plot of ln (intensity) versus inverse temperature for two duraldehyde in durene bands

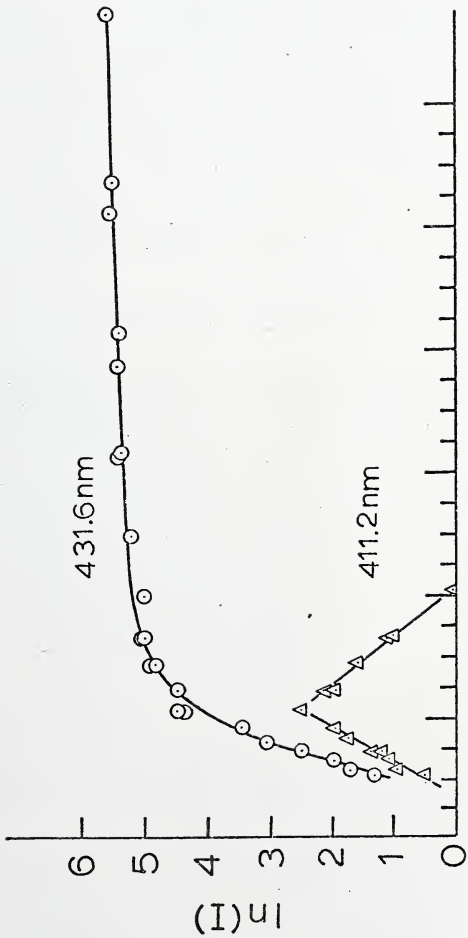
431.6nm
411.2nm
ln(I)
0
1
2
3
4
5
6
12
24
36
48
60
72
1/T×10³(K⁻¹)

Figure 25. Plot of ln (intensity) versus temperature for two duraldehyde in in durene bands

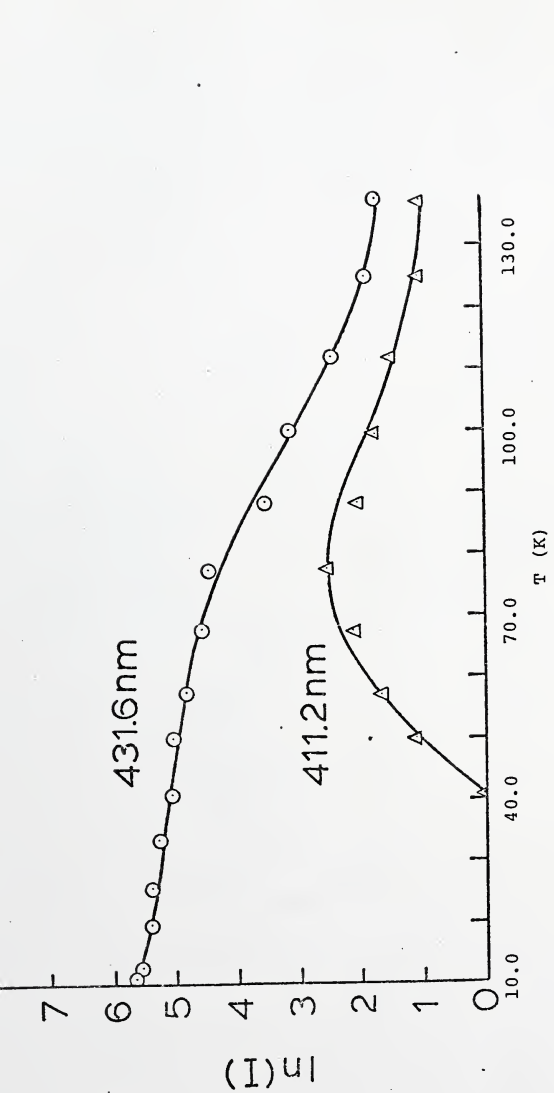
431.6nm
411.2nm
ln(I)
T (K)
10.0
40.0
70.0
100.0
130.0
0
1
2
3
4
5
6
7

results although at temperatures below 90-100K it was not possible to reliably monitor the decay of the new emission bands. Decays were exponential in two regions: from 11 to about 95K and above 110K. Between 95 and 110K the results were nonexponential. Results for the exponential decays generally show a standard deviation of 1 to 3% with 99% confidence limits. The results for the short-lived component of the nonexponential decay are probably in error by as much as 30% for runs at 110K because of its small contribution to the total decay intensity at these temperatures. Figure 26 is a plot of lifetime versus temperature for our results while Figure 27 is a plot of the natural logarithm of the decay rate versus inverse temperature for the same data. Lifetime results between 11 and 27K show a small temperature dependence while results between 30 and 60K are essentially constant.

Infrared Results

Figure 28 shows the infrared spectra of duraldehyde in durene in the 1650-1800 cm^{-1} range at various temperatures. The bands in the 1743-1759 cm^{-1} region of the spectra are probably overtone and combination bands of the 450 and 860 cm^{-1} vibrations of durene. By use of crystals with low concentrations of duraldehyde, we were able to show that the two bands at 1685 cm^{-1} and 1703 cm^{-1} are due to duraldehyde. The intensity of these two peaks relative to each other and relative to the lower-lying durene bands indicate that their relative concentrations are temperature independent.

Figure 26. Plot of lifetime versus temperature for duraldehyde in durene
Curve A = Low temperature results
Curve B = High temperature results

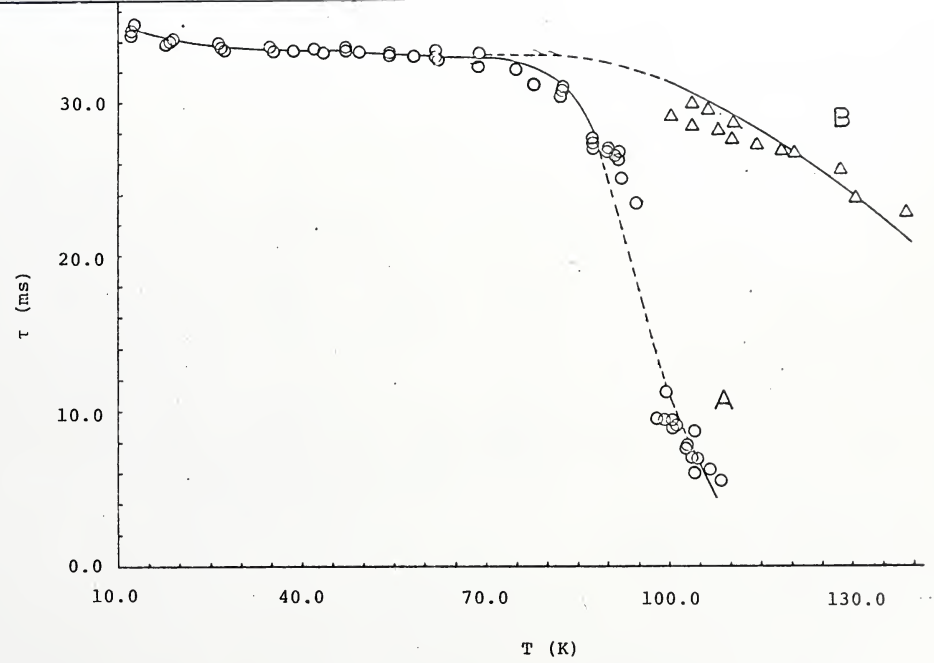
30.0
20.0
10.0
0.0
τ (ms)
10.0
40.0
70.0
100.0
130.0
T (K)
A
B

Figure 27. Plot of ln (decay rate) versus inverse temperature for duraldehyde in durene

Curve A = Low temperature results

Curve B = High temperature results

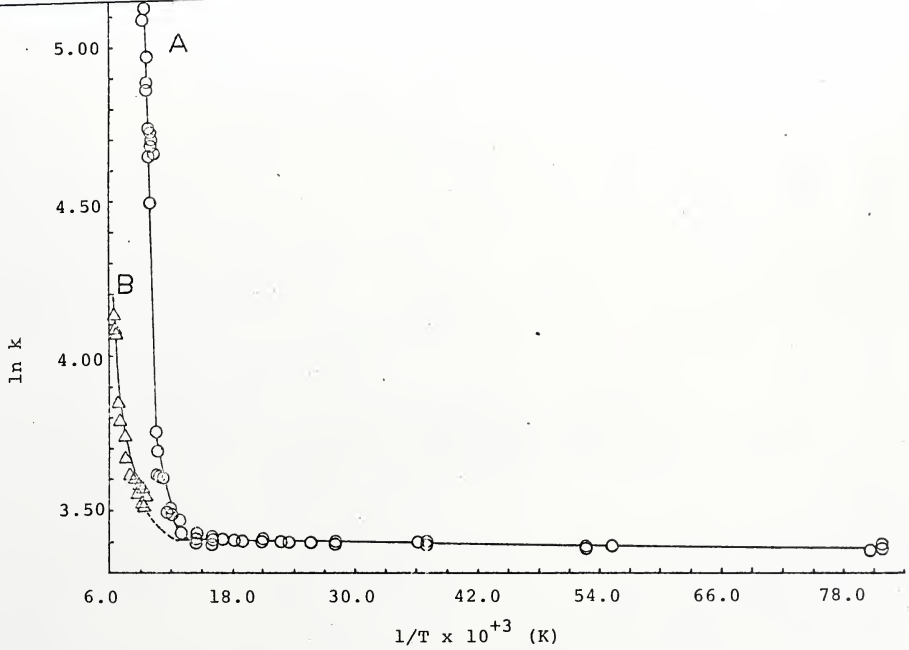
5.00
4.50
4.00
3.50
ln k
A
B
6.0
18.0
30.0
42.0
54.0
66.0
78.0
1/T x 10+3 (K)

Figure 28. Temperature dependence of the infrared spectrum of duraldehyde in durene for the 1650 → 1800 cm^{-1} region

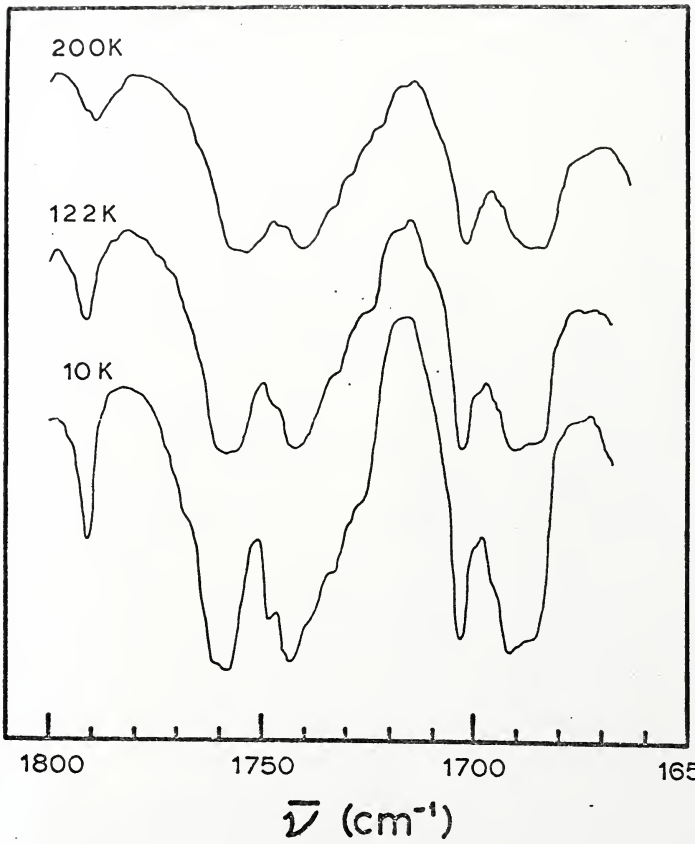
200K
122K
10K
1800
1750
1700
1650
$\bar{\nu}$ (cm^{-1})

Figure 29 illustrates the effects of photolysis on infrared band intensities. Irradiation at 80-120K for a period of one hour had no effect on the 85K spectrum shown in the figure. Irradiation at 160-180K for a similar period had some effect on the 1703 cm^{-1} band but no apparent effect on the 1685 cm^{-1} band. A second hour of irradiation in this temperature range further decreased the intensity of the 1703 cm^{-1} band (Figure 29). An additional hour of irradiation between 200 and 240K produced the most drastic effect of all on the 1703 cm^{-1} band while there was, at most, a small change in the 1685 cm^{-1} band (see Figure 29). Thus, photolysis, especially at high temperatures, has a significant effect on the concentration of the species exhibiting the 1703 cm^{-1} carbonyl stretching frequency.

Discussion

Phenomenological Model

We propose that the phosphorescence, photochemical and infrared results of duraldehyde in durene can best be understood from a model (see Figure 30) in which there are two inequivalent duraldehyde molecules in the durene lattice, each with its own unique photochemical and photophysical behavior. The possible existence of two inequivalent duraldehyde molecules in the durene lattice may be inferred from the durene crystal structure. Substitution of a CHO group for a CH_3 group may occur in either of the two environmentally inequivalent methyl sites on the same molecule or on crystallo-

Figure 29. Effect of irradiation on the infrared spectrum (1650 → 1800 cm^{-1} region) of duraldehyde in durene

Bottom - No irradiation at 85K

Middle - 2 hours irradiation at 160-180

Top - 1 hour additional irradiation at 200-240K

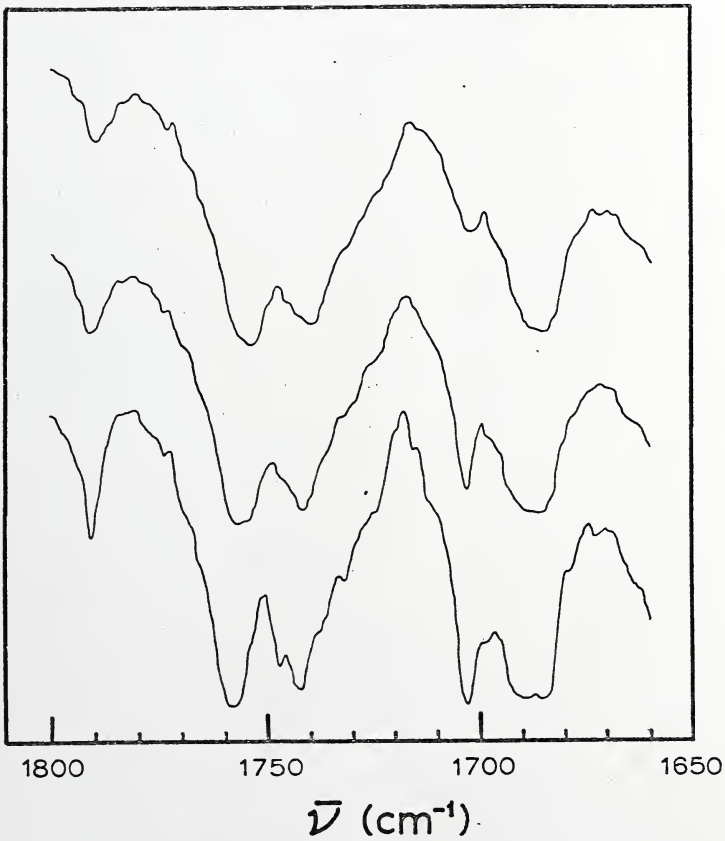
1800
1750
1700
1650
$\bar{\nu}$ (cm^{-1})

Figure 30. Phenomenological model of the duraldehyde in durene system

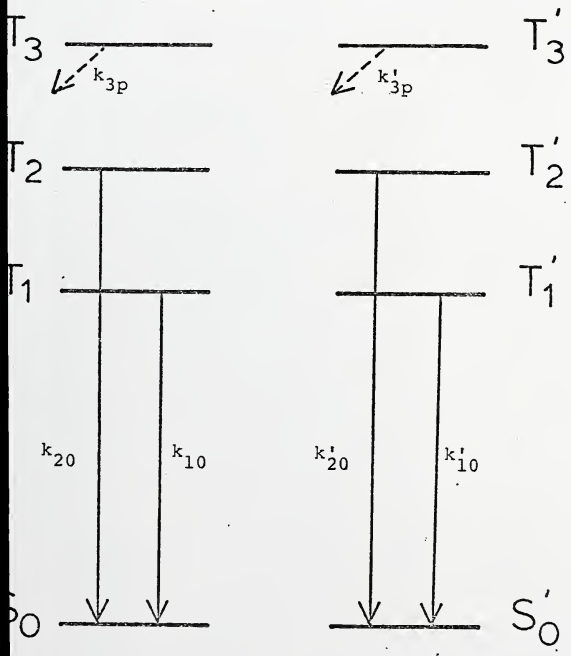
T3
k3p
T2
T1
k20
k10
S0
T'3
k'3p
T'2
T'1
k'20
k'10
S'0

graphically inequivalent molecules. Three different experimental results point to existence of two inequivalent duraldehydes: 1) our infrared results showing two bands in the carbonyl stretching region; 2) the low temperature phosphorescence spectrum showing a 23 cm^{-1} doubling of most bands;[73] and 3) the triplet state ESR results showing two signals.[74]

The two high energy temperature dependent phosphorescence bands at 408.0 nm and 411.2 nm which grew in with temperature belong to two different emitting species as can be seen from their different temperature dependencies. The two bands appear at very different temperatures (56K for the 408.0 nm band versus 40K for the 411.2 nm band) and have nearly equal relative intensities by 146K. A clear qualitative interpretation of these results is complicated by the fact that at high temperatures the intensity of the 411.2 nm band (which has shifted to 411.8 nm) results from a vibration built on the 408.0 nm origin; the energy difference between the 408.0 nm band and the high temperature 411.8 nm band is 226 cm^{-1}, a value in agreement with a 204 cm^{-1} mode observed by Fischer. At low temperatures before the onset of the 408.0 nm band, emission at 411.2 nm must be due to a different species.

To compensate for the apparent overall decrease in phosphorescence intensity with temperature increase (see Figure 25), we considered the intensities of the two new bands relative to the low temperature origin band at 413.8 nm.

Since phosphorescence intensities are equal to the product of the radiative rate and the population of the state and since the relative population of two states (T_1: 413.8 nm; T_2: 408.0 nm or 411.2 nm) is given by:

$$[T_2] = [T_1]e^{-\Delta E_{21}/kT} \tag{17}$$

we obtain

$$I_2/I_1 = k_2^r[T_2]/k_1^r[T_1] = k_2^r e^{-\Delta E_{21}/kT}/k_1^r \tag{18}$$

where k_1^r and k_2^r are the radiative rate constants for phosphorescnece from states T_1 and T_2, respectively, and ΔE_{21} is the energy difference between these two states. Figure 31 shows a plot of $\ln(I_2/I_1)$ versus 1/T for both the 408.0 nm and 411.2 nm band intensities relative to the 413.8 nm band intensity. A linear least-squares fit for the slopes of these plots gave $\Delta E = 200 \pm 10$ cm^{-1} for the 411.2 nm band ($\Delta E_{21} = 180 \pm 20$ cm^{-1} if the 431.6 nm band is used instead of the 413.8 nm band) and $\Delta E_{21} = 420 \pm 50$ cm^{-1} for the 408.0 nm band. The expected values for ΔE_{21} based on the energy separation of the phosphorescence bands is 160 cm^{-1} for the 411.2 nm band and 400 cm^{-1} for the 408.0 nm band, in good agreement with the above results. That the results show as little deviation as they do is surprising as the emission from the 413.8 nm band is a sum of emission intensities from two steps. It will later be shown that at low temperatures the emission is predominantly from one site while at high temperatures it is predominantly from the other. This

Figure 31. Plot of ln (I_2/I_1) versus inverse temperature

I_2 = New emission bands

I_1 = Low temperature emission bands

—— = 413.8 nm band used for I_1

--- = 431.6 nm band used for I_1

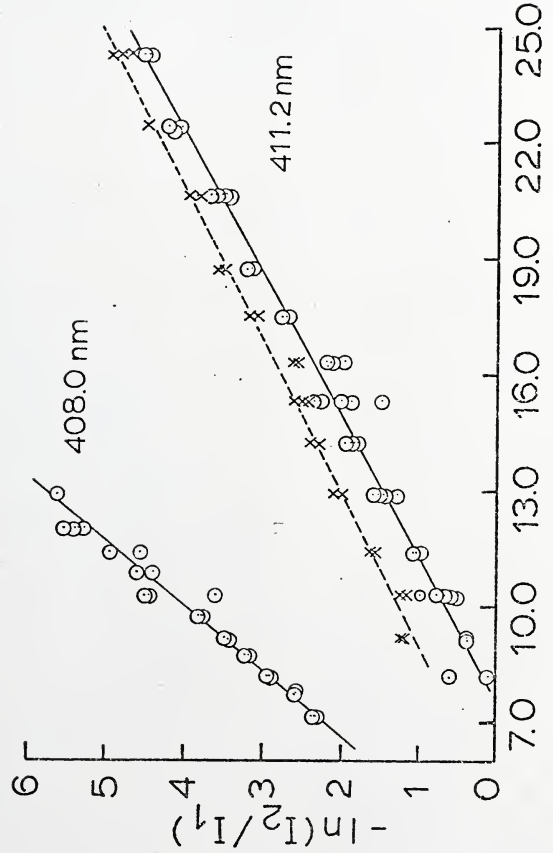
408.0 nm
411.2 nm
$-\ln(I_2/I_1)$
$1/T \times 10^3 (K^{-1})$
0
1
2
3
4
5
6
7.0
10.0
13.0
16.0
19.0
22.0
25.0

explains why at high temperatures the 411.2 nm band results show the most scatter while the opposite is true for the 408.0 nm band. The intercepts from Figure 31 also give the ratio $\frac{k_2^r}{k_1^r}$ for the 411.2 nm band as 9.2±0.6 (4.3±0.5 if the 431.6 nm band is used instead of the 413.8 nm band) while for the 408.0 nm band the value is 57±6.

It is well known from Migirdicyan's work that two photoproducts are formed in this system. That each of the photoproducts is produced from a different site can be seen from the present lifetime results.

Lifetime Results

From our phenomenological model we can now understand why the lifetime results change from exponential to nonexponential and back to exponential. At low temperatures the duraldehyde molecules in each site are emitting with very similar lifetimes and hence the decays appear to be exponential. This is reasonable as the site effect is small and should not have a drastic effect on lifetimes. At some higher temperature (about 77K) additional processes come into play where the site effect can play a significant role. This causes the molecules in the different sites to have different lifetimes and the emission thus becomes nonexponential. In a somewhat higher temperature region a radiationless process associated with one of the sites becomes a great deal faster than the other, the net result of which is that the emission intensity from this site becomes very small and the decay

from this site becomes so fast (relative to the other state) that it can no longer be observed. We are thus left with emission from one site and an apparent exponential decay.

There are two major observations which argue in favor of a thermal equilibrium process between a lower and upper triplet rather than a thermal activation process as the intensity gaining mechanism for the high energy 408.0 nm and 411.2 nm bands. First, as a comparison of Figures 24 and 27 show, there is no change in the observed lifetime in the 40-77K region where the 408.0 nm and the 411.2 nm bands grow in intensity with temperature. A change is expected for a thermal activation mechanism. Secondly, no nonexponentiality is observed in any of the phosphorescence decays in this range as is theoretically predicted for a thermal activation process.

For a thermal equilibrium process we have from equations (8) and (9) that the observed decay rate, k, is:

$$k = \frac{k_{10} + k_{20} e^{-\Delta E_{21}/kT}}{1 + e^{-\Delta E_{21}/kT}} \qquad (19)$$

For $\Delta E_{21} = 160\ cm^{-1}$, no change in the observed lifetime is expected, provided k_{20} is less than a factor of two greater than k_{10}. This requires that the lifetime of the 411.2 nm band be about 20ms, a value which is long for a pure $^3n\pi^*$ state, but reasonable for a triplet $n\pi^*$ with some $\pi\pi^*$ character. Because of the larger energy difference, the lifetime of the 408.0 nm band can be as short a 1ms without

producing any effect on the lifetime results. This value is consistent with a pure $^3n\pi^*$ emissive state.

In addition to the thermal equilibrium between two sets of two triplets which originate from two inequivalent duraldehyde molecules, it is necessary to hypothesize an additional radiationless process which drains each of these sets of triplets in order to account for the dual drop-off in lifetime with increasing temperature (see Figure 26). We postulate the formation of two different photoproducts via a thermal activation mechanism from each of the two inequivalent duraldehydes. For each duraldehyde, an expression for k_{20} now including the photoproduct formation can be written as:

$$k_{20} = k'_{20} + k^{\circ}_{23} e^{-\Delta E_{32}/kT}$$

where k'_{20} is the low temperature decay rate from state T_2, and the second term gives the rate of photoproduct formation. Substituting this expression into equation (19) for the observed rate gives:

$$k = \frac{k_{10} + k'_{20} e^{-\Delta E_{21}/kT} + k^{\circ}_{23} e^{-(\Delta E_{21} + \Delta E_{32})/kT}}{1 + e^{-\Delta E_{21}/kT}} \qquad (20)$$

Since $k'_{20} e^{-\Delta E_{21}/kT}$ is small and $\Delta E_{21} + \Delta E_{32} = \Delta E_{31}$, equation (20) can be rewritten:

$$k = \frac{k_{10} + k^{\circ}_{23} e^{-\Delta E_{31}/kT}}{1 + e^{-\Delta E_{21}/kT}} \qquad (21)$$

The form of this expression is similar to that used to fit the temperature dependence of the benzene phosphorescence

lifetimes in the first part of this dissertation (see Tables 2 and 3). The results for a series of fits to equation (21) are shown in Table 10. The solid lines in Figures 26 and 27 are the calculated fits using form III (see Table 10). The correspondence between the calculated fit and the experimental data is shown in Table 11. The major results from these fits are the values found for the activation energies, ΔE_{31}. For the low temperature fit (curve A in Figures 26 and 27) an activation energy of 1200 cm^{-1} was found which is in good agreement with the 1400 cm^{-1} energy required for photoenol production in the lower temperature range.[84] For the high temperature fit (curve B in Figures 26 and 27) an activation energy of 540 cm^{-1} was determined. This value is in excellent agreement with both the activation energy for duryl radical formation (600 cm^{-1})[83] and photoenol formation in the higher temperature region (560 cm^{-1}).[84] These results confirm our hypothesis of thermal activation of a photoproduct (photoenol and duryl radical) as the major mechanism of lifetime shortening with temperature increase and support our contention that there are two inequivalent duraldehyde molecules in the durene lattice each with its own photophysical and photochemical energy dissipation processes.

Kinetic Model

From the above experimental results, we propose the model shown in Figure 32 to account for the primary photochemical and photophysical processes of duraldehyde in

Table 10
Parameters Determined from Observed Decay Rates for Duraldehyde in Durene

Curve	Form	k_{10} (s^{-1})	k°_{23} (s^{-1})	ΔE_{31} (cm^{-1})
A	I	30.1 ± .3	(1.3 ± 1.0) x 10^{+9}	1180 ± 60
A	II	30.6 ± .4	(4.9 ± 3.5) x 10^{+8}	1100 ± 50
A	III	30.0	(1.2 ± 0.8 x 10^{+9}	1170 ± 50
A	IV	30.0	(2.9 ± 1.9) x 10^{+8}	1060 ± 50
B	I	30.2 ± .3	5500 ± 2200	550 ± 40
B	II	30.2 ± .3	5700 ± 2200	550 ± 40
B	III	30.0	4900 ± 2300	540 ± 50
B	IV	30.0	5100 ± 1700	540 ± 30

Form I $k = k_{10} + k^{\circ}_{23} e^{-\Delta E_{31}/kT}$

Form II $k = \dfrac{k_{10} + k^{\circ}_{23} e^{-\Delta E_{31}/kT}}{1 + e^{-\Delta E_{21}/kT}}$

$\Delta E_{21} = 160\ cm^{-1}$ curve A

Form III $k = C_{10} + k^{\circ}_{23} e^{-\Delta E_{31}/kT}$

Form IV $k = \dfrac{C_{10} + k^{\circ}_{23} e^{-\Delta E_{31}/kT}}{1 + e^{-\Delta E_{21}/kT}}$

$\Delta E_{21} = 400\ cm^{-1}$ curve B

Table 11
Sample Fit to Duraldehyde Decay Rates
(Form III)

Temperature (K)	Experimental Rates (s^{-1})	Calculated Rates (s^{-1})	Percentage Deviation
	Low Temperature Results (Curve A)		
27.5	29.8	30.0	0.4
35.4	29.8	30.0	0.6
35.5	29.7	30.0	0.9
38.7	29.9	30.0	0.2
42.2	29.7	30.0	0.7
43.9	29.9	30.0	0.2
47.3	29.9	30.0	0.3
47.3	29.8	30.0	0.6
49.7	29.9	30.0	0.0
54.5	30.1	30.0	-0.5
54.6	30.1	30.0	-0.4
58.7	30.3	30.0	-1.0
62.1	30.5	30.0	-1.6
62.2	29.9	30.0	0.3
62.3	30.1	30.0	-0.7
69.0	30.8	30.0	-2.7
69.3	29.8	30.0	0.5
69.3	29.9	30.0	0.1
75.3	31.0	30.1	-2.6
75.3	29.6	30.2	2.1
78.2	32.0	30.5	-4.8
82.6	32.2	31.7	-1.7
82.7	32.4	31.7	-2.1
82.7	32.9	31.7	-3.8
82.7	32.2	31.7	-1.5
82.7	32.6	31.7	-2.8
82.7	32.3	31.7	-1.9
87.8	36.5	35.6	-2.4

Table 11 - continued

Temperature (K)	Experimental Rates (s^{-1})	Calculated Rates (s^{-1})	Percentage Deviations
87.8	36.6	35.6	-2.8
87.9	36.1	35.7	-1.1
88.0	36.9	35.9	-2.8
90.3	37.3	39.6	5.9
90.3	37.3	39.6	6.0
92.1	38.2	43.8	14.6
92.1	37.3	43.8	17.2
92.5	40.0	44.9	12.2
94.7	42.7	52.7	23.5
98.2	105.	72.8	-31.0
99.4	105.	82.7	-21.3
99.5	89.1	83.6	-6.2
100.9	112.	97.7	-13.1
101.0	110.	98.9	-10.4
101.0	108.	98.9	-8.0
102.9	131.	124.	-6.1
102.9	129.	124.	-4.6
104.2	170.	145	-14.8
107.1	162.	208.	28.0
108.6	184.	251.	36.5
	High Temperature Results (Curve B)		
101.0	34.4	32.2	-6.6
104.2	34.7	32.7	-5.7
104.3	33.4	32.8	-2.0
107.1	33.9	33.4	-1.6
110.9	36.0	34.3	-4.8
110.9	34.8	34.3	-1.4
113.4	38.6	35.1	-7.6
113.4	36.9	35.1	-5.1
113.5	39.6	35.1	-11.4

Table 11 - continued

Temperature (K)	Experimental Rates (s^{-1})	Calculated Rates (s^{-1})	Precentage Deviation
114.9	36.6	35.5	-2.8
119.1	37.1	37.0	-0.4
120.7	37.4	37.7	0.8
120.7	40.4	37.7	-6.6
123.2	37.4	38.8	3.6
128.6	39.1	41.4	6.1
130.9	42.1	42.7	1.6
139.2	44.1	48.2	9.2
141.9	46.9	50.2	6.9
142.0	47.6	50.3	5.7
148.6	59.1	55.9	-5.5
150.5	62.4	57.7	-7.7
151.2	65.5	58.3	-10.9

Figure 32. Kinetic model of the duraldehyde in durene system

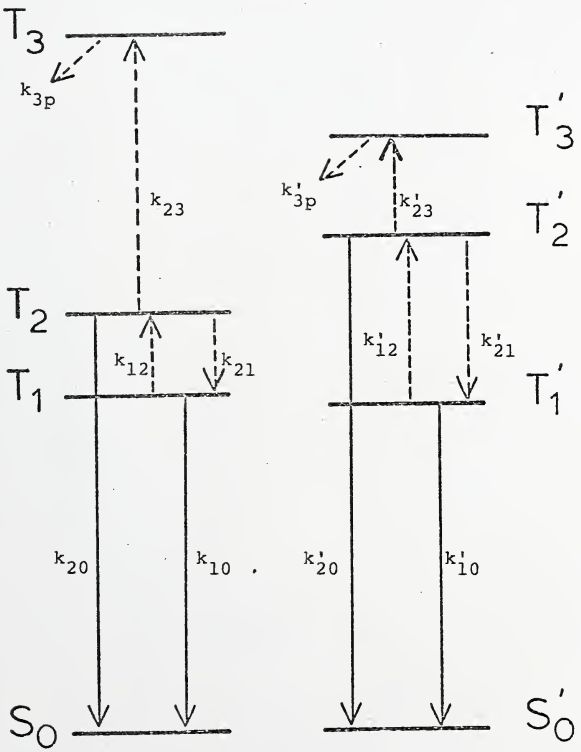
T3
k3p
k23
T2
k12
k21
T1
k20
k10
S0
T'3
k'3p
k'23
T'2
k'12
k'21
T'1
k'20
k'10
S'0

durene. The key to the interpretation of the experimental results lies in the presence of two inequivalent sets of duraldehyde molecules, each with its own particular radiationless processes. In one set (the unprimed one) low temperature emission emanates solely from the T_1 state (413.8 nm) while at higher temperatures (beginning at 40K) emission from the T_2 state (411.2 nm) becomes observable and finally at still higher temperatures (~80K) intramolecular photoenol product formation commences, resulting in the precipitous shortening of the phosphorescence lifetime with increasing temperature (curve A, Figure 27). In the other set (primed), low temperature emission occurs from the T_1' state which is 23 cm^{-1} lower in energy than the T_1 (413.8 nm) state of the first set. The simultaneous emission from both T_1 and T_1' of two inequivalent duraldehyde molecules accounts for the doubling of the low temperature phosphorescence spectrum observed by Fischer and confirmed by us. Emission from the T_2' state (408.0 nm) commences at ~65K and at higher temperatures intermolecular photoenol/duryl radical formation sets in. The latter process accounts for the decline in the lifetime (curve B, Figure 27) with increasing temperature.

The following rate equations can adequately describe the process for either sets of molecules as outlined in Figure 32. Either site may then be described by the following set of equations (see Figure 32):

$$\frac{d[T_1]}{dt} = k_{ISC}[S_1] - (k_{10} + k_{12})[T_1] + k_{21}[T_2] \qquad (22)$$

$$\frac{d[T_2]}{dt} = k_{12}[T_1] - (k_{20} + k_{21} + k_{23})[T_2] \quad (23)$$

$$\frac{d[T_3]}{dt} = k_{23}[T_2] - k_{3p}[T_3] \quad (24)$$

Under steady-state conditions these equations may be solved to give:

$$[T_1] = \frac{k_{ISC}[S_1](k_{20} + k_{21} + k_{23})}{(k_{10}+k_{12})(k_{20}+k_{21}+k_{23})-k_{12}k_{21}} \quad (25)$$

$$[T_2] = \frac{k_{ISC}[S_1]k_{12}}{(k_{10}+k_{12})(k_{20}+k_{23}+k_{21})-k_{12}k_{21}} \quad (26)$$

$$[T_3] = \frac{k_{23}}{k_{3p}}[T_2] \quad (27)$$

k_{10}, k_{20} and k_{3p} are temperature independent rates while k_{23} is temperature dependent and can be represented by an Arrhenius-type term (i.e., $k_{23} = k_{23}^{\circ}e^{-\Delta E_{32}/kT}$). k_{21} and k_{12} are related by the thermal equilibrium condition ($k_{12} = k_{21}e^{-\Delta E_{21}/kT}$) where k_{21} may be taken as temperature independent for the regions of interest. Substitution of these temperature dependent forms into equation (26) gives:

$$[T_2] = \frac{k_{ISC}[S_1]k_{21}}{(k_{10}e^{\Delta E_{21}/kT})(k_{20}+k_{21}+k_{23}^{\circ}e^{-\Delta E_{32}/kT})-k_{21}^2} \quad (28)$$

A test of the validity of our model can be made by using the heretofore determined kinetic parameters in the steady state solution for T_2 (equation (28)) and ascertaining whether its rather unusual temperature dependence can be predicted. The

known parameters are:

$\Delta E_{21} = 160\ cm^{-1}$; $\Delta E_{31} = 1200\ cm^{-1}$

$\Delta E_{32} = \Delta E_{31} - \Delta E_{21} = 1000\ cm^{-1}$

$k_{10} = 30.0\ s^{-1}$

$k_{23}^{\circ} = 1.2 \times 10^{9}\ s^{-1}$

$k_{20} = 50\ s^{-1}$

We know that $k_{21} >> k_{20}$ (for thermal equilibrium) and is here assumed to be $k_{21} = 1 \times 10^{5}\ s^{-1}$ although changing the parameter to $1 \times 10^{+9}\ s^{-1}$ was not found to effect the results. $k_{ISC}[S_1]$ is taken as an adjustable parameter which is varied to match the observed phosphorescence intensity at 80K, the curve maximum. With $k_{ISC}[S_1] = 4200$ the fit shown in Figure 33 for the 411.2 nm band is determined. The calculated curve drops off too rapidly at higher temperatures, but this is most likely due to the band overlap prevalent in this temperature range which renders the measured experimental intensities for the 411.2 nm band too large. The too-rapid intensity increase on the low temperature edge of the calculated curve appears to be due to the overall phosphorescence intensity decrease with temperature increase as observed particularly clearly for the 413.8 and 431.6 nm bands (see Figures 24 and 25 for a plot for the latter band). The decrease in intensity with temperature for this band (431.6 nm) is too rapid to be explained solely on the basis of the present model. If, however, a process such as thermally-activated internal conversion in the first excited singlet

Figure 33. Theoretical fit to the variation of the 411.2 nm band intensity with temperature

--- Without singlet process

—— With singlet process

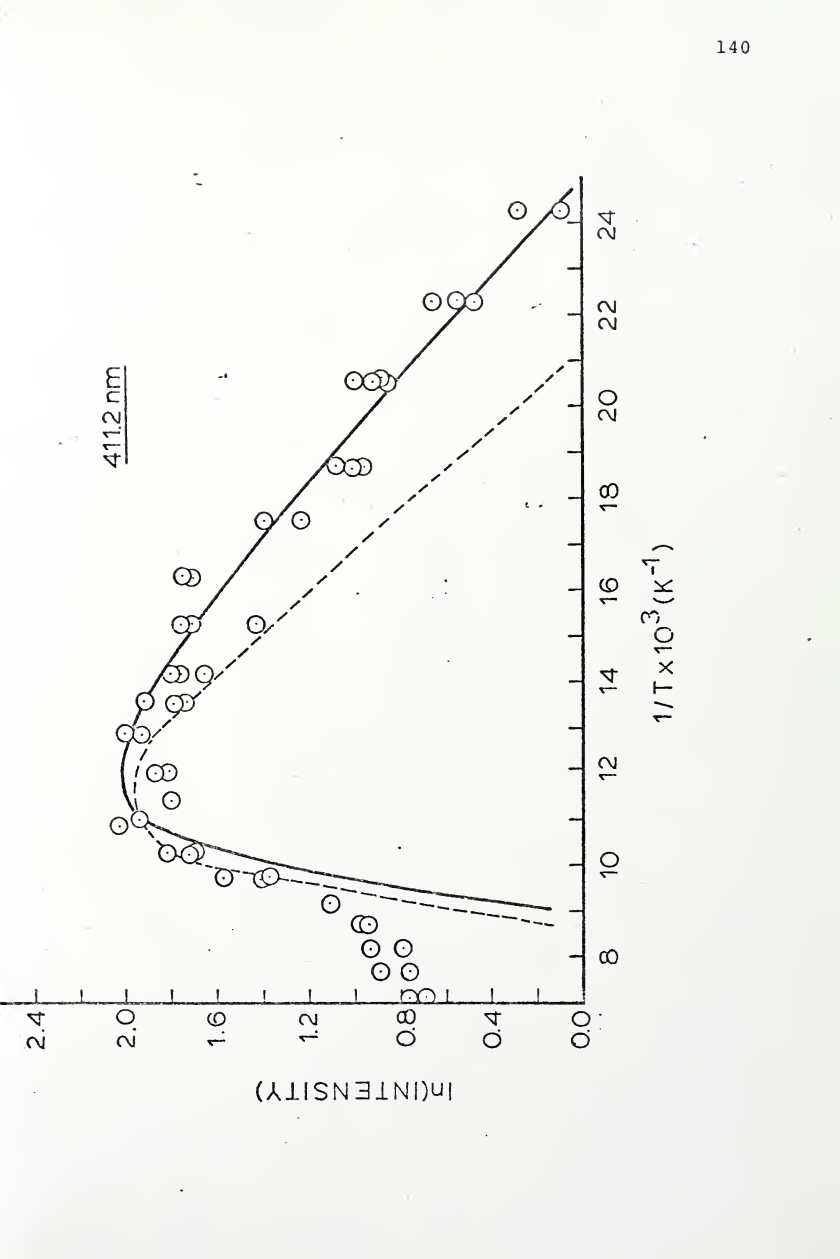
411.2 nm
ln(INTENSITY)
2.4
2.0
1.6
1.2
0.8
0.4
0.0
8
10
12
14
16
18
20
22
24
1/T x10^3 (K^-1)

state were to occur, then the rate of intersystem crossing to T_1 (or T_1') is given not by $k_{ISC}[S_1]$ as originally, but by $c\left(\frac{k_{ISC}}{k_{ISC}+\alpha k_{ISC}e^{-\Delta E_s/kT}}\right)$ or more simply: $c(1+\alpha e^{-\Delta E_s/kT})^{-1}$ where c is a constant, ΔE_s the activation energy for this process and α the number of times faster the new dissipative rate is compared to the original. For a ΔE_s of 100 cm^{-1}, c = 12000, and α = 10, the improved fit to the 411.2 nm band shown by the solid line in Figure 33 is obtained.

In order to effect a fit to the 431.6 nm band intensities it is necessary to account for the emission from both T_1 and T_1' states in the two sites. Using the following known parameters for the primed set of molecules:

$\Delta E'_{21}$ = 400 cm^{-1}

$\Delta E'_{32}$ = 140 cm^{-1}

k'_{10} = 30.0 s^{-1}

$k^{o}{}'_{23}$ = 5 x 10^3 s^{-1} $\qquad$ k'_{20} = 1000 s^{-1}

with k'_{21} the same as in the first set and the relative intensities from the two sites in the ratio 4:1 (unprimed to primed set with I_o = 4000) from Fischer's low temperature results,[73] the fit to the 431.6 nm band shown in Figure 34 is obtained. The dashed curve is the fit (properly normalized to the same low temperature intensity) without the singlet process and the solid curve is with the singlet process included. It can be seen that the fit with the singlet process included is much superior. It is gratifying that the fit with the singlet process is as good as it is since the

Figure 34. Theoretical fit to the variation of the 431.6 nm band intensity with temperature

--- Without singlet process

—— With singlet process

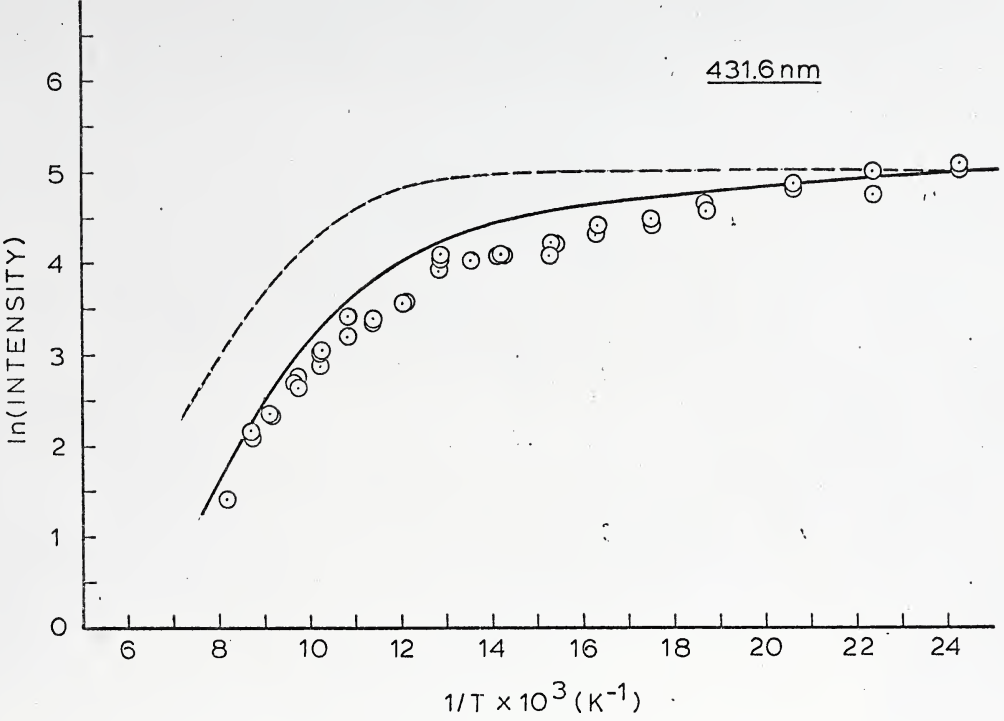
431.6 nm
ln(INTENSITY)
0
1
2
3
4
5
6
6
8
10
12
14
16
18
20
22
24
1/T x 10^3 (K^-1)

parameters used were not optimized for emission from the primed site. Substituting the above mentioned parameters for the primed system into the expression for T_2 (c = 25,000) results in a correct prediction of the overall temperature dependence of the 408.0 nm band intensity (see Figure 35). Because of its low phosphorescence intensity for all temperatures, the experimental scatter is large compared to that for the 411.2 nm band. Since the calculated fit does not appear to be sensitive to most of the parameters, and furthermore, since there is no real criterion for choosing one fit over another, an optimized fit has not been attempted.

A close inspection of the temperature dependence of the 413.8 nm or 431.6 nm bands (Figure 24) reveals that there are at least three processes which contribute to its intensity behavior with temperature and that their contributions are different in the different temperature ranges. The first dominates in the 30 to 60K range and is responsible for the gentle decline in the intensity in this region. This process may correspond to the singlet internal conversion process discussed above. The second process, which controls the drastic intensity decline in the 70 to 100K range, is predominantly the thermal activation process to the intramolecular photoenol. Since the 411.2 nm state intensity becomes very small at 100K and since the 413.8 nm state in the unprimed set is in equilibrium with it, the 413.8 nm band intensity must also fall sharply. Interestingly though, the observed

Figure 35. Theoretical fit to the variation of the 408.0 nm band intensity with temperature

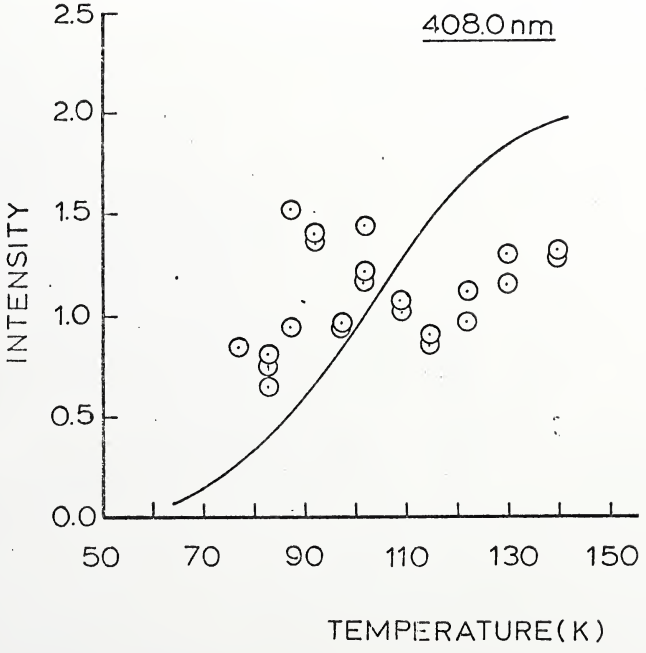
408.0 nm
INTENSITY
2.5
2.0
1.5
1.0
0.5
0.0
50
70
90
110
130
150
TEMPERATURE(K)

413.8 nm band intensity does not drop off at the temperature that the 411.2 nm band does. The reason is that the third process, emission from the primed set of duraldehydes, now becomes dominant at temperatures above 100K, not declining in intensity as rapidly as that from the unprimed set.

It is now possible to understand why the plots of ln (I_2/I_1) versus 1/T for both 408.0 nm and 411.2 nm bands give good straight lines with accurate values for the activation energies even though the 413.8 nm band is a composite emission from both sites. At low temperatures, emission at 413.8 nm from the unprimed sites dominates, whereas at high temperatures emission in the same region from the primed sites dominates. Thus, the ratio I_2(411.2 nm)/I_1(413.8 nm) samples emission from predominantly the unprimed sites at lower temperatures and the ratio I_2(408.0 nm)/I_1(413.8 nm) samples emission from predominantly the primed sites at higher temperatures. In Figure 36 is shown the predicted ratio of ln (I_2/I_1) at several temperatures where emission is expected from all three bands using the above mentioned parameters. In addition, the emission intensity of the 408.0 nm band has been added to the 411.2 nm band intensity in the 70-110K temperature range to account for the fact that a vibration from the 408.0 nm origin overlaps the latter band in this temperature range. Intensities are as chosen previously and have not been optimized to give the best results.

Figure 36. Predicted behavior for a plot of $\ln \left(\frac{I_2}{I_1}\right)$ versus inverse temperature

I_2 = Predicted intensity of new emission band

I_1 = Predicted intensity of 431.6 nm emission band

—— = Approximate fit to predicted points

--- = Approximate experimental slope if different from predicted slope

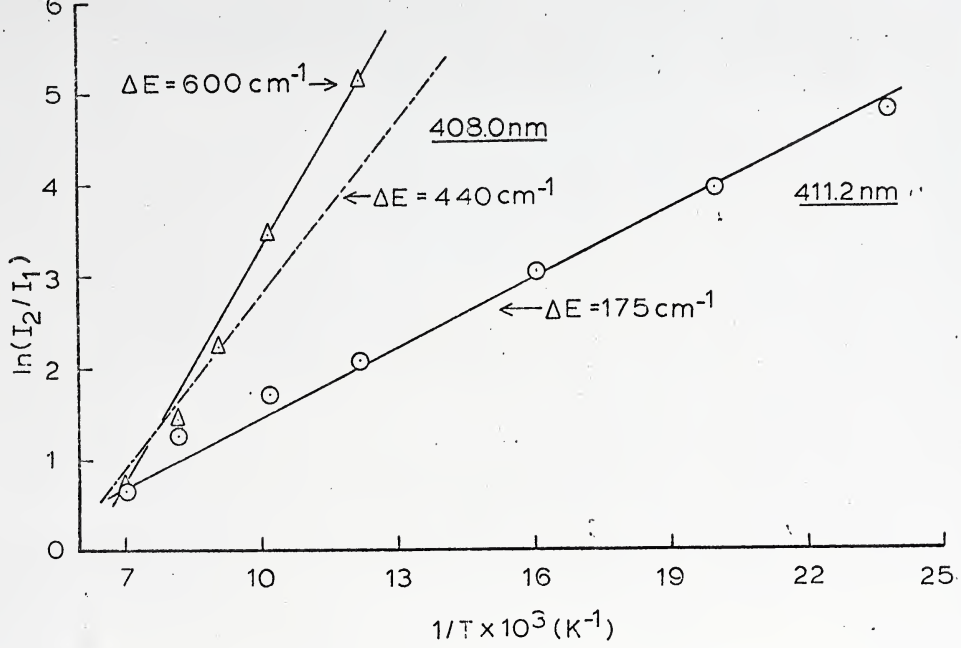
ΔE = 600 cm-1
408.0nm
←ΔE = 440 cm-1
411.2 nm
←ΔE = 175 cm-1
ln(I2/I1)
1/T x 10^3 (K-1)
0
1
2
3
4
5
6
7
10
13
16
19
22
25

Infrared Results

The temperature independence of the carbonyl stretching intensities at 1703 cm^{-1} and 1685 cm^{-1} over the range 10-300K indicates that there is no ground state thermal equilibrium between the two species exhibiting these vibrations, and that the species are independent and inequivalent. The low temperature (4K) phosphorescence spectrum of duraldehyde in durene reveals one quantum of a 1684 cm^{-1} vibration built on the 413.8 nm T_1 (unprimed) origin. It is therefore reasonable to equate the 1684 cm^{-1} species to those duraldehydes in the unprimed sites. Fischer did not report seeing any band corresponding to the 1703 cm^{-1} vibration. Our phosphorescence results show that the emission from the second (primed) set is not only weaker but also substantially broadened indicating that it might not have been observed. Nevertheless, we equate the 1703 cm^{-1} band to those duraldehydes in the primed sites. One piece of evidence supports this claim. At higher temperatures upon ultraviolet irradiation the species exhibiting the 1703 cm^{-1} mode gradually disappears. Since duryl radical and intermolecular photoenol are apparently formed in larger quantities at higher temperatures than the intramolecular photoenol and since our primed system shows the proper activation energy for the formation of these products, it is reasonable that this set of duraldehydes correspond to the 1703 cm^{-1} species. (*Vide infra* for a rationale for the irradiation independence of the 1684 cm^{-1} species.)

Identification of Emitting Species

We propose that the species corresponding to the T_1, T_2, and T_3 states in each type of site are as shown in Figure 37. The primary emitter at low temperatures (40K and below) is the E-type isomer whose carbonyl group lies in-plane and oriented away from the adjacent methyl. Sharnoff's ESR results indicate such a conformation for both inequivalent species. As mentioned in the durene crystal structure section, the environment about the methyls on the durene are inequivalent; in particular, the number and length of the intermolecular distances from adjacent durene hydrogens to the two in-plane hydrogens are different. One of these hydrogens has no near-neighbor close "contacts" while the other has. If the aldehyde group of the duraldehyde were to substitute for each of these methyls with the carbonyl in-plane, it would account for the observed differences. The primed, more intense set would then occupy the site with no near-neighbor close "contacts" and the unprimed set the other. This is reasonable since the duraldehydes in the primed sets undergo carbonyl group rotation to form the intramolecular photoenol, whereas the duraldehydes in the primed sites with close contacts (~2.7 Å) to neighboring durene hydrogens undergo intermolecular photoenol and simultaneous duryl radical formation.

State T_2 of the unprimed site is identified as the lowest triplet of the Z-isomer formed from the rotation of the

Figure 37. Comprehensive model for the duraldehyde in durene system

T3
T2
411.2
413.8
T1
S0
T'3
T'2
408.0
414.2
T'1
S'0

carbonyl group of the E-isomer. This out-of-plane rotation will cause an interchange in the ordering of the triplet levels. The lowest triplet of the E-isomer is predominantly $^3\pi\pi^*$, although it must contain some $n\pi^*$ character as evidenced by its short (33ms) phosphorescence lifetime. Upon rotation of the aldehyde group, however, the stabilization of the $^3\pi\pi^*$ state is decreased drastically because of the loss of conjugation between the aromatic ring and the carbonyl group and the lowest triplet of the newly-created Z-isomer becomes a $^3n\pi^*$. It is well known that formation of photoenols proceeds very efficiently via hydrogen abstraction in triplet $n\pi^*$ states.[87,88] Thus, the formation of the intramolecular photoenol of duraldehyde via the $^3n\pi^*$ state of the precursor Z-isomer is reasonable. The photoenol thus formed may not be very stable,[89] however, and may readily revert back to the aldehyde. If true in the present system, this would explain the relative independence to u.v. irradiation exhibited by the 1684 cm^{-1} infrared band. The intramolecular photoenol may have been formed upon irradiation, but simply reverted back to the aldehyde form in the time it took to run the i.r. experiments.

For the primed site, state T_2' is identified as the lowest triplet $n\pi^*$ of a conformer formed by the rotation of the carbonyl group (and possibly the reorientation of the entire duraldehyde in the lattice site). The rotation is thought to occur only partially to some out-of-plane position in

which the carbonyl is correctly positioned with respect to a near-neighbor durene methyl group to undergo intermolecular hydrogen abstraction. Concomitant with the formation of the photoenol will be the formation of a duryl radical and a hydrogen atom. The state T_3' then corresponds to the triplet state of the intermolecularly formed photoenol. That both the intramolecular photoenol and duryl radical are formed simultaneously is supported by their similar activation energies, 540 cm^{-1} and 600±80 cm^{-1}, respectively, as measured by Migirdicyan in separate investigations. It is interesting that Migirdicyan observed two different activation energies for the formation of photoenol and that the lower activation energy process (540 cm^{-1}) appears in the higher temperature range (215-300K).[84] This result is understandable if the duryl and intermolecular photoenol are formed simultaneously. It has been shown that duryl radical formation requires an induction period before observation which decreases with temperature increases and, therefore, for simultaneous production of photoenol and duryl, the photoenol should also. Since Migirdicyan plotted the initial rate of photoenol formation versus 1/T, the 540 cm^{-1} process would not appear until the temperature was high so that the induction period was short.

The intermolecular process apparently forms a photoenol which is more stable than the intramolecular one. The infrared irradiation results indicate that the 1703 cm^{-1} species

decreases with prolonged photolysis at higher temperatures. If the intermolecular photoenol were formed in such a conformation that reversion to the aldehyde were difficult, the decrease in concentration of its E-isomer precursor would be understandable. Possibly relaxation of the intermolecular photoenol to a planar conformation with the hydroxyl group oriented away from the adjacent methylene can occur rapidly before reversion. In this conformation, the photoenol is no doubt the most stable.

The reasons for the induction period for photoenol/duryl formation are not clear but the calculated preexponential factor for this process is only 5×10^3 s^{-1} compared to the 1.2×10^9 s^{-1} found for the intramolecular process. The low value may be related to this induction period.

The proposal made above that the rotation of the carbonyl group requires only 160 cm^{-1} in one site and only 400 cm^{-1} in the other requires some discussion. These energies represent differences between equilibrium conformations and do not represent the potential barrier height to rotation. Although we have assumed in our kinetic model that k_{21}, the rate constant for back rotation (i.e., from the Z- to the E-isomer in the unprimed site), is temperature independent; this assumption implies that the barrier height and the energy difference between equilibrium conformations is the same. It is not a key assumption to the understanding of the general intensity behavior of either the T_1 or T_2 states in

either site, and may, in fact, be changed without undermining the major proposals made here.

Comments on Other Aromatic Carbonyls

Dual phosphorescence has been claimed to have been observed in a number of aromatic carbonyls.[80,90-92] The sensitivity of the order of the lower-lying triplets to environment is now well documented.[90,92-96] Current theories interpret the dual phosphorescence in these systems to be the result of a small energy gap between the $^3\pi\pi^*$ and $^3n\pi^*$ states of the same molecule. Because of the small gap, there is a small density of states at the second triplet level so that there results a relatively low probability of radiationless decay between the two triplets and competitive radiative decay from the upper triplet is thought to occur. While this interpretation may be correct for some systems, it is not applicable to the duraldehyde in durene system, where different conformers are the different emitters. It is our belief that a number of other aromatic carbonyls should be reinvestigated in light of the results given here.

BIBLIOGRAPHY

1. E. Wiedemann, Ann. Phys., 34, 446 (1888).

2. A. Jablonski, Z. Physik, 94, 38 (1935).

3. G. N. Lewis and M. Kasha, J. Am. Chem. Soc., 66, 2100 (1944).

4. G. N. Lewis and M. Calvin, J. Am. Chem. Soc., 67, 1232 (1945).

5. C. A. Hutchinson, Jr. and B. W. Magnum, J. Chem. Phys., 29, 952 (1958).

6. S. P. McGlynn, T. Azumi, and M. Kinosheta, Molecular Spectroscopy of the Triplet States, Prentice-Hall, Inc., Englewood Cliffs, New Jersey, 1969.

7. M. Kasha, Disc. Faraday Soc., 9, 14 (1950).

8. B. DiBartolo, Optical Interactions in Solids, John Wiley, New York, New York, 1968, pp. 442-446.

9. S. H. Lin, J. Chem. Phys., 56, 2648 (1972).

10. D. Mahoney, Ph.D. Dissertation, Anomalous Phosphorescent Emission and Nonexponential Decay in Aromatic Carbonyl Compounds, Univ. of Florida, 1974, Appendix.

11. H. Shull, J. Chem. Phys., 17, 295 (1949).

12. A. C. Albrecht, J. Chem. Phys., 38 354 (1963).

13. G. C. Nieman and D. S. Tinti, J. Chem. Phys., 46, 1432 (1967).

14. M. S. de Groot and J. H. van der Waals, Mol. Physics, 6, 545 (1963).

15. D. S. McClure, J. Chem. Phys., 17, 905 (1949).

16. H. Gilmore, G. E. Gibson, and D. S. McClure, J. Chem. Phys., 20, 829 (1952).

17. E. C. Lim, J. Chem. Phys., 36, 3497 (1962).

18. M. R. Wright, R. P. Frosch, and G. W. Robinson, J. Chem. Phys., 33, 934 (1960).

19. P. G. Russell and A. C. Albrecht, J. Chem. Phys., 41, 2536 (1964).

20. T. E. Martin and A. H. Kalantar, J. Phys. Chem., 72, 2265 (1968).

21. G. C. Nieman, G. F. Hatch, and M. D. Erlitz, Molecular Luminescence, E. C. Lim, ed., W. A. Benjamin, New York, New York, 1969, pp. 21-38.

22. I. H. Leubner and J. E. Hodgkins, J. Phys. Chem., 73, 2545 (1969).

23. I.H. Leubner, J. Phys. Chem., 74, 77 (1970).

24. N. G. Kilmer and J. D. Spangler, J. Chem. Phys., 54, 604 (1971).

25. G. W. Robinson and R. P. Frosch, J. Chem. Phys., 38, 1187 (1963).

26. M. Gouterman, J. Chem. Phys., 36, 2846 (1962).

27. F. H. Mies and M. Kraus, J. Chem. Phys., 45, 4455 (1967).

28. S. H. Lin, J. Chem. Phys., 44, 3759 (1966).

29, S. Fischer, Chem. Phys. Letters, 10, 397 (1971).

30. D. Chock, J. Jortner, and S. A. Rice, J. Chem. Phys., 49, 610 (1968).

31. D. Haaland, Ph.D. Dissertation, Triplet State of Benzene and its Methyl Derivatives, Univ. of Rochester, 1973, pp. 104-112.

32. G. C. Nieman, M. D. Erlitz, and G. F. Hatch, J. Chem. Phys., 49, 3723 (1968).

33. M. S. de Groot, I. A. M. Hesselman, and J. H. van der Waals, Mol. Phys., 10, 91 (1965).

34. D. Bryce-Smith and H. C. Longuet-Higgins, Chem. Comm., 593 (1966).

35. K. E. Wilzbach, A. L. Harkness, and L. Kaplan, J. Am. Chem. Soc., 90, 1116 (1968).

36. G. E. Gibson, N. Blake, and M. Kalm, J. Chem. Phys., 21, 1000 (1953).

37. S. Leach and E. Migirdicyan, J. Chim. Phys., 54, 643 (1957).

38. S. Leach and E. Migirdicyan, J. Chim. Phys., 58, 409 (1961).

39. S. Leach and E. Migirdicyan, J. Chim. Phys., 58, 416 (1961).

40. S. Leach and E. Migirdicyan, J. Chim. Phys., 58, 762 (1961).

41. E. Migirdicyan, J. Chim. Phys., 63, 520 (1966).

42. E. Migirdicyan, J. Chim. Phys., 63, 535 (1966).

43. E. Anderson, H. T. J. Chilton, and G. Porter, Proc. Chem. Soc., 352 (1960).

44. E. Migirdicyan, J. Chim. Phys., 63, 543 (1966).

45. S. Leach, E. Migirdicyan, J. Chim. Phys., 56, 749 (1959).

46. B. N. Shelimov, N. V. Fok, and V. Voevodskii, Dokl. Akad. Nauk. SSSR, 144, 483 (1962).

47. V. G. Vinogradova, B. N. Shelimov, N. V. Fok, and V. V. Voevodskii, Dokl. Akad. Nauk. SSSR, 154, 12 (1964).

48. V. G. Vinogradova, L. M. Baider, B. N. Shelimov, and N. V. Fok, Dokl. Adad. Nauk. SSSR, 168, 290 (1966).

49. T. S. Zhuravlyeva, Opt. Spec., 25, 696 (1968).

50. J. P. Simons and N. C. Perrins, Trans. Faraday Soc., 65, 390 (1969).

51. C. J. Creswell and A. L. Allred, J. Phys. Chem., 66, 1949).

52. N. C. Perrins, J. P. Simons, and A. L. Smith, Trans. Faraday Soc., 67, 3415 (1971).

53. J. P. Simons and A. L. Smith, Chem. Phys. Letters, 16, 536 (1972).

54. J. P. Simons and A. L. Smith, J. Chem. Soc., Faraday Trans. II, 70, 53 (1974).

55. J. P. Simons and A. L. Smith, Chem. Phys. Letters, 25, 97 (1974).

56. D. M. Haaland and G. C. Nieman, J. Chem. Phys., 59, 1010 (1973).

57. J. Baiardo, Department of Chemistry, Univ. of Florida, (unpublished).

58. G. C. Nieman, J. Chem. Phys., 50, 1674 (1969).

59. R. W. Rabalais, H. J. Maria, and S. P. McGlynn, J. Chem. Phys., 51, 2259 (1969).

60. P. Dobosh, Program CNINDO, #141 from the Quantum Chemistry Program Exchange.

61. J. A. Pople, D. L. Beveridge, Approximate Molecular Orbital Theory, McGraw-Hill, Inc., New York, New York, 1970.

62. M. Barrow, Introduction to Molecular Spectroscopy, McGraw-Hill, Inc., New York, New York, 1962, p. 283.

63. G. P. Semeluk and I. Unger, Nature, 198, 853 (1963).

64. I. Unger and G. P. Semeluk, Can. J. Chem., 44, 1427 (1966).

65. S. H. Ng, G. P. Semeluk, and I. Unger, Can. J. Chem., 46, 2459 (1963).

66. J. A. Stone and P. T. Dyne, Radiation Res., 17, 353 (1962).

67. J. K. Thomas and I. Mani, J. Chem. Phys., 51, 1834 (1969).

68. W. V. Sherman, Advances in Free Radical Chemistry, Vol. 3, G. H. Williams, ed., Academic Press, New York, New York, 1969, pp. 1-82.

69. R. B. Cundall and D. A. Robinson, Chem. Phys. Letters, 14, 438 (1972).

70. I. H. Leubner, private communication.

71. Y. Meyer and R. Astier, J. Phys. (Paris), 24, 1089 (1963).

72. H. Sponer and Y. Kanda, J. Chem. Phys., 40, 778 (1964).

73. G. Fischer, Mol. Cryst. Liquid Cryst., 11, 85 (1970).

74. M. Sharnoff, Mol. Cryst., 5, 297 (1969).

75. S. J. Sheng and D. M. Hanson, J. Chem. Phys., 60, 368 (1974).

76. S. W. Mao and N. Hirota, Mol. Phys., 27, 309 (1974).

77. T. H. Cheng and N. Hirota, Chem. Phys. Letters, 13, (1974).

78. T. H. Cheng and N. Hirota, Mol. Phys., 27, 281 (1974).

79. T. H. Cheng and N. Hirota, J. Chem. Phys., 56, 5019 (1972).

80. S. W. Mao and N. Hirota, Mol. Phys., 27, 327 (1974).

81. T. H. Cheng, Ph.D. Dissertation, ESR and Spectroscopic Studies of Triplet States of Aromatic Carbonyl Compounds, State Univ. of New York at Stony Brook, 1972.

82. E. Migirdicyan, Chem. Phys. Letters, 12, 473 (1971).

83. E. Migirdicyan, J. Chem. Phys., 55, 1861 (1971).

84. E. Migirdicyan, A. Despres, V. Lejuene, and S. Leach, J. Photochem., 3, 383 (1975).

85. J. M. Robertson, Proc. Roy. Soc., Ser. A, 141, 594 (1933).

86. C. H. Stam, Acta Crystallogr., Sect. B, 28, 2630 (1972).

87. G. Porter and M. F. Tchir, J. Chem. Soc., Ser. A, 23, 3772 (1971).

88. M. B. Ledger and G. Porter, J. Chem. Soc., Faraday Trans. I, 68, 539 (1972).

89. M. Dewar and R. Dougherty, The PMO Theory of Organic Chemistry, Plenum Press, Inc., New York, New York, 1975, p. 458.

90. N. Kanamaru, M. E. Long, and E. C. Lim, Chem. Phys. Letters, 26, 1 (1974).

91. M. E. Long, Y. H. Li, and E. C. Lim, Mol. Photochem., 3, 221 (1971).

92. L. Goodman and M. Koyanagi, Mol. Photochem., 4, 369 (1972).

93. J. B. Gallivan and J. S. Brinen, Chem. Phys. Letters, 10, 455 (1971).

94. J.B. Gallivan, Can. J. Chem., 50, 3601 (1972).

95. M. Koyanagi and L. Goodman, J. Chem. Phys., 57, 1809 (1972).

96. M. Koyanagi, R. Zwarich, and L. Goodman, J. Chem. Phys., 56, 3044 (1972).

BIOGRAPHICAL SKETCH

William Emil Moehle was born in Long Island City, New York, on May 1, 1948. He graduated cum laude from Queens College of the University of the City of New York in June, 1969, with a Bachelor of Arts in Science degree. Since that time he has been enrolled in the Graduate School of the University of Florida. He has held National Science Foundation Traineeships and a Graduate Council Fellowship. He is a member of Phi Beta Kappa and the American Chemical Society.

I certify that I have read this study and that in my opinion it conforms to acceptable standards of scholarly presentation and is fully adequate, in scope and quality, as a dissertation for the degree of Doctor of Philosophy.

Martin T. Vala, Chairman
Associate Professor of Chemistry

I certify that I have read this study and that in my opinion it conforms to acceptable standards of scholarly presentation and is fully adequate, in scope and qualtiy, as a dissertation for the degree of Doctor of Philosophy.

William Weltner, Jr.
Professor of Chemistry

I certify that I have read this study and that in my opinion it conforms to acceptable standards of scholarly presentation and is fully adequate, in scope and quality, as a dissertation for the degree of Doctor of Philosophy.

Willis B. Person
Professor of Chemistry

I certify that I have read this study and that in my opinion it conforms to acceptable standards of scholarly presentation and is fully adequate, in scope and quality, as a dissertation for the degree of Doctor of Philosophy.

Thomas L. Bailey
Professor of Physics

I certify that I have read this study and that in my opinion it conforms to acceptable standards of scholarly presentation and is fully adequate, in scope and quality, as a dissertation for the degree of Doctor of Philosophy.

Charles P. Luehr
Assistant Professor of Mathematics

This dissertation was submitted to the Graduate Faculty of the Department of Chemistry in the College of Arts and Sciences and to the Graduate Council, and was accepted as partial fulfillment of the requirements for the degree of Doctor of Philosophy.

December, 1975

Dean, Graduate School

39